# Deflection of a dilute stream of particles

Yu Hui Deng,* Jonathan J. Wylie,† and Qiang Zhang‡
*Department of Mathematics, City University of Hong Kong, 83 Tat Chee Avenue, Kowloon Tong, Hong Kong*
(Received 21 October 2009; revised manuscript received 21 April 2010; published 29 July 2010)

We consider a two-dimensional system in which a dilute stream of particles collides with an oblique planar wall. Both collisions between particles and collisions between particles and the wall are inelastic. We perform numerical simulations in two dimensions and show that the mean force experienced by the wall can be a nonmonotonic function of the angle between the wall and the particle stream. We show that this occurs because particles that rebound from the wall can collide with incoming particles and be scattered. This kind of particle-particle collision can reduce the force experienced by the wall. We refer to this effect as shielding. Furthermore, we show that the force experienced by the wall may be an increasing, decreasing or nonmonotonic function of the restitution coefficient in particle-particle collisions. We derive an exact solution for the mean force on the wall if the system is dilute, and the theoretical prediction is found to be in good agreement with our numerical results. The theory allows us to explicitly quantify the effects of shielding, and thus to explain a number of interesting features. The theory generally provides a useful upper bound for the mean force.

DOI: 10.1103/PhysRevE.82.011307 PACS number(s): 45.70.−n

## I. INTRODUCTION

In this paper we consider the mechanisms that underlie the process of deflection when a dilute granular stream collides with a rigid wall. By a granular stream, we mean a localized stream of discrete moving particles with small random transverse fluctuating velocities. We will consider the case in which collisions between particles and collisions between particles and the wall are characterized by a loss of energy. We will show that this seemingly simple system can give rise to an array of surprising dynamics.

There is a broad range of industrial applications in which streams of particles interact inelastically with rigid boundaries. Industrial devices designed for the purposes of particle handling may have objectives such as diverting particle streams or reducing the kinetic energy of the particles. Alternatively, devices may be designed for the purpose of cleaning or abrading a surface, as in the case of sand blasting. In such applications, details of the dynamics of the particles and the forces experienced by the particles are critical for understanding how these objectives can be best achieved. Other important applications are related to powerful natural hazards such as rock falls, debris flows and avalanches. In order to mitigate risks from these natural hazards, passive protection methods are often employed to deflect or absorb the kinetic energy of the flows. Examples of this include the metal containment nets that are widely used above roads, boulder-gathering trenches that are dug at the base of hills and barriers that attempt to deflect flows around critical populated areas. Unfortunately, the dynamics of these flows present numerous conceptual, theoretical and technical difficulties. This means that the design of passive protection methods often does not have a solid theoretical underpinning [1]. A solid understanding of the deflection of granular flows would clearly represent an important advance in this regard.

The problems of classical fluid impinging on obstacles have been studied by many authors. Peng and Parker [2] studied a two-dimensional free-surface problem of an ideal fluid impinging on an uneven wall. They obtained a relation between the flow angle on the free surface and the wall angle. Wiryanto and Tuck [3] considered a steady two-dimensional free-surface flow in a channel impinging on a vertical wall with finite height. The stream is found to go upward and it may split into two jets. The problem of a steady flow emerging from a nozzle, hitting a horizontal plate and falling under gravity was considered by Christodoulides and Dias [4]. The plate can either divert the stream or lead to detachment.

Granular materials share many similarities with classical fluids, and thus exhibit some analogous behavior. For example, Anderson elucidated in his book [5] that shocks can occur when supersonic flows are deflected by a wedge. A similar phenomena also occurs in granular materials [6]. Other examples of these similarities are found in certain impact problems. When liquid droplets impact on a flat liquid surface narrow vertical fluid jets are formed by the radial collapse of the liquid "craters" produced by the impacting rain drops [7]. Thoroddsen and Shen [8] considered the case of a solid sphere impacting on a deep layer of granular material. They showed that similar narrow jets occur for granular materials.

However, the presence of dissipation during particle collisions for granular particles represents an essential difference with classical fluids [9]. Consequently granular materials also exhibit some different phenomena from those observed in classical fluids. Amarouchene and Kellay [10] performed experiments with granular materials and found the features such as Mach cones and shock wave detachment that are also observed in supersonic molecular fluids under extreme conditions. They also showed that, in contrast to classical fluids, the velocity distributions for granular materials are far from being Gaussian and display algebraic tails. Royer *et al.* [11] showed that, in contrast to jets formed by impacts in fluids, the jets formed in granular materials are composed of two separate components, an initial thin jet formed by the collapse of the cavity left by the impacting

*ivandengyh@gmail.com
†mawylie@cityu.edu.hk
‡mazq@cityu.edu.hk

 

object stacked on top of a second, thicker jet which depends strongly on the ambient gas pressure. They also found that the interstitial gas played two distinct roles in the formation of the jet. The problem of impact craters formed by dropping a steel ball vertically into a container of small glass beads was studied by Walsh *et al.* [12] and de Vet and de Bruyn [13]. They showed that these impact craters are very nearly hyperbolic in profile, and both the diameter and the depth of the craters are dependent on the impact energy, as well as the projectile density and size.

Due to the distinct phenomena exhibited by granular flows the understanding of how granular flows interact with rigid boundaries has been considered in a number of important studies. Given the importance of these problems, it is not surprising that there has been a significant amount of experimental work. Rericha *et al.* [14] showed that shocks can form when a stream of particles collides with a rigid wedge. Cheng *et al.* [15] performed experiments in which a stream of particles collided with a fixed object. They showed that wide incoming streams could result in thin sheets or cones of outgoing particles that were similar in shape to analogous flows in zero-surface-tension liquids. Tuzun and Nedderman [16,17] have performed experiments involving interactions between slowly moving particles and objects. They showed that stagnation zones can form upstream of the obstacle and void regions downstream of the obstacle.

There has also been a number of studies focusing on the force during the interaction between granular flows and rigid boundaries. Wieghardt [18] studied the situation in which momentum transfer between particles is dominated by sustained particle contacts and the force is dominated by frictional interactions. He dragged an array of rods through a bed of sand and found that the force varied slowly as the speed of the rod varied. Chehata *et al.* [19] considered the dense granular flow past an immersed cylinder. They showed that the effective force on the cylinder is strongly affected by the surrounding channel geometry. Zik *et al.* [20] considered the flow of energetic particles past an object. They dragged a sphere through a vibrofluidized granular bed. They showed that force depended strongly on the speed of the particle and that systems with highly energetic particles behave in a completely different way to systems that are dominated by friction such as the experiments described above. Wassgren *et al.* [21] considered the dynamics of a cylinder placed in the path of a stream of particles. They effectively considered the case in which the width of the particle stream is much larger than the size of the cylinder. They used a discrete element method to simulate a two-dimensional flow and hence computed the effective force on the cylinder.

In the above studies, the focus was principally on the case in which the obstacle is of comparable size or much smaller than the width of the flow. The focus of this paper is the deflection of avalanches or jets and therefore we will consider the opposite case in which the width of the flow is much smaller than the size of the obstacle.

Hákonardóttir and Hogg [22] considered the interaction of granular flows with deflecting dams. They performed experimental studies and developed a theoretical framework to describe free-surface flows. The shallow-layer limit considered by these authors averages the flow properties over the depth of the layer and gives a set of equations for the bulk flow. In our study, we will consider the interaction at the particle level to understand the dynamics of the deflection process at a different scale.

Fang *et al.* [23] considered the motion of a single particle falling through a funnel composed up of two rigid walls and found that the time that the particle spends in the funnel is a complicated function of the funnel angle. The collapse phenomena of a particle in a corner formed by two boundaries has been studied by Gao *et al.* [24]. In bidisperse particle systems, the case of shocks induced by a moving boundary was considered by Wylie *et al.* [25]. Wylie and Zhang [26] showed that phase-locking and complicated orbits collapse occur for dissipative particle systems that are driven by forcing from a boundary. Wylie *et al.* [27] and Wylie *et al.* [28] studied the motion of a large number of particles in a closed box that are excited by a vibrating boundary and experience a linear drag force from the interstitial fluid.

In this paper, we will focus on the effective force experienced by the rigid boundary and show that a number of surprising phenomena can occur in dilute systems. The study of dilute systems provides a number of important insights into the qualitative behavior of denser systems. In Sec. II, we will formulate the problem. In Sec. III, we will perform numerical simulations in two dimensions and show that the effective force can be a nonmonotonic function of the angle between the particle stream and the boundary. We also show that the effective force can be either an increasing, decreasing or nonmonotonic function of the restitution coefficient in particle-particle collisions. In this section we will show that the surprising behavior is present in the case in which most of the particles experience relatively few collisions. We will therefore develop a dilute theory that can give good agreement with the simulations in Sec. IV and study the validity of our theory in Sec. V. In Sec. VI, we will explain the above-mentioned phenomena by using our theory.

## II. FORMULATION

We consider a system in which a dilute stream of particles originating from infinity collides with an oblique planar wall of infinite length (see Fig. 1). We assume that the stream consists of identical smooth spheres of radius $a$ and mass $m$. We further assume that all incoming particles move in the same direction and have the same initial velocity $v_0$. The angle between the wall and the direction of the stream is $\theta$. We will consider a two-dimensional system, but the methodology explained in this paper can be extended to three dimensions in a straightforward way. We will discuss this in Sec. IV. We define axes with the $Y$ axis parallel to the stream, and the $Z$ axis perpendicular to the stream.

Collisions between particles are inelastic with a constant restitution coefficient $0 \leq e \leq 1$. Here the coefficient of restitution is defined as the ratio of the relative velocities of two particles in the direction along their line of centers immediately after and immediately before the particle-particle collision. The coefficient of restitution is assumed to be independent of velocity and denotes the degree of dissipation in particle collisions. Collisions between particles and the wall

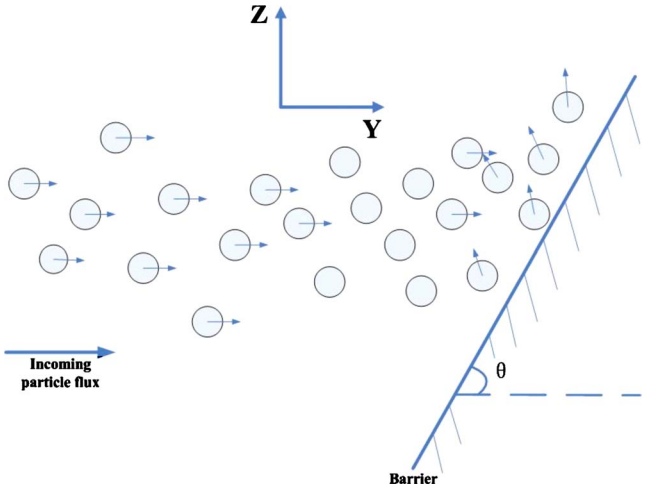


FIG. 1. (Color online) The system we consider.

are also inelastic with restitution coefficient $0 \leq e_w \leq 1$, which is defined as the ratio of the relative velocities of particles to the wall immediately after and before the particle-wall collision.

The particles in the stream are randomly located, and in general, the spatial distributions of particles in the directions parallel and perpendicular to the stream will be different. We now specify the statistics of the relative particle locations within the stream. Without loss of generality, we assume that the coordinate system is chosen so that the mean $Z$ location of particles is zero. We denote the marginal density function of the $Z$ location of particles as $\rho_Z$ and the standard deviation of $\rho_Z$ as $\sigma_Z$. We denote the marginal density function of the distance in the $Y$ direction between adjacent particles as $\rho_Y$. Here by adjacent particles, we mean two particles that are closest in $Y$ direction, even though they are not necessarily closest in terms of Euclidean distance. We denote the mean of $\rho_Y$ as $\mu_Y$. We note that for dense particle streams in which the magnitude of $\mu_Y$ is comparable with the particle radius $a$ there will be strong dependence between the locations of particles since two particles cannot occupy the same location. However, for the relatively dilute particle streams we will consider in this paper, the dependence will be weak.

We will begin by neglecting gravity and will consider the effects of gravity in Sec. VI and show that the surprising phenomena that occurs for systems with negligible gravity also can exist when gravity is non-negligible.

The system can be described by the following parameters: the deflector angle $\theta$, the particle-particle restitution coefficient $e$, the particle-wall restitution coefficient $e_w$, the two distributions $\rho_Y$ and $\rho_Z$, and two dimensionless parameters $V=\frac{\mu_Y}{a}$ and $S=\frac{\sigma_Z}{a}$. The parameters $V$ and $S$, respectively, indicate the particle denseness in $Y$ direction and $Z$ direction. We denote the effective mean force experienced by the oblique wall as $F_{mean}$. That is, $F_{mean}$ is defined as the average impulse experienced by the wall per unit time. Then we will consider the dimensionless force $f_{mean}=\frac{F_{mean}}{mv_0^2/\mu_Y}$ which represents the average dimensionless impulse on the wall per particle in the stream.

## III. NUMERICAL RESULTS

In our numerical simulations, rather than considering particle streams originating from infinity, we consider a finite domain that is much larger than $\mu_Y$ and $\sigma_Z$. Particles enter the system at the left boundary of the domain. When particles leave the domain, they are removed and cannot re-enter the domain. If, when a new particle enters the system it overlaps with any previous particles, then this particle is removed. Since we focus on dilute particle streams, there are typically few such particles. For our numerical simulations we choose $\rho_Z$ to be a Gaussian distribution with standard deviation $\sigma_Z$. For simplicity, we choose $\rho_Y$ to be nonrandom, that is, all particles are spaced $\mu_Y$ apart in the $Y$-direction. As we will show at the end of Sec. IV, relaxing this assumption and including randomness does not qualitatively affect the phenomena we present in the paper.

We also note that in numerical simulations the inclusion of small random fluctuating velocities at the inlet does not fundamentally affect the qualitative behavior described in this paper. In particular, the nonmonotonic phenomena for the mean force still exists. However, the case of particles with equal initial velocity lends itself to a theoretical treatment that can elucidate the important underlying mechanisms.

The algorithm to propagate particles is composed of two methods. The first is a collision detection method that treats particles as hard spheres and assumes that particle collisions are binary events. In this case, the results of collisions can be solved explicitly and the method computes the times that each pair of particles would collide if no other particles were present, then it selects the minimum of these times and uses the collision rules to update the position and velocity of the particles. This strategy is then repeated. This method resolves collisions very rapidly and efficiently and is very well suited for relative dilute systems. Nevertheless, this method cannot always work when inelastic collapse [29] occurs and an infinite number of collisions occur in a finite time. In this case, when the time between collisions is below a threshold we use another method that employs soft spheres to model the individual particles in the system. Particle collisions are considered to occur over a finite time with a potential force that each individual particle experiences with its surrounding particles. The magnitude of the force is given by

$$|Force| = \begin{cases} W \exp\left(\frac{d}{\epsilon} - \frac{\varepsilon}{d}\right) & \text{if } d > 0 \text{ and } \dot{d} \geq 0 \\ e^2 W \exp\left(\frac{d}{\epsilon} - \frac{\varepsilon}{d}\right) & \text{if } d > 0 \text{ and } \dot{d} < 0 \\ 0 & \text{if } d \leq 0 \end{cases},$$

where $d$ is the overlap distance, $\dot{d}$ is the rate of change of $d$ with respect to time, $W$ is the strength of the force and $\varepsilon$ is the length over which the force increases. The direction of the force is assumed to be along the line of centers of the two particles. If after a time step there are no interactions between particles, the algorithm reverts to the collision detection method. The mixture of the two methods provides a robust and efficient algorithm for our numerical simulations.

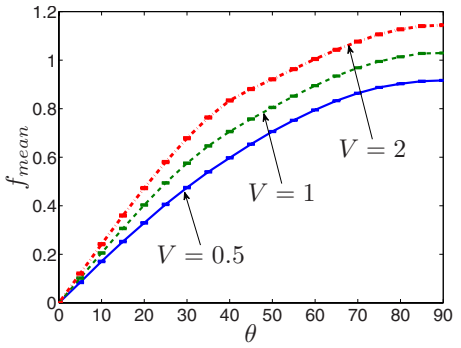


FIG. 2. (Color online) The mean force $f_{mean}$ versus the deflector angle $\theta$ in dense particle streams for $V$=0.5 (solid blue), $V$=1 (dashed green) and $V$=2 (dot dashed red). Other parameters are $S$=20 and $e$=$e_w$=0.8. The mean force is a monotonically increasing function of $\theta$.

One may naively imagine that the larger the angle $\theta$ is, the larger the velocity component in the direction perpendicular to the wall, and thus the wall experiences a larger force. This is true in a dense particle stream such as the case shown in Fig. 2. The figure shows that in a dense particle stream the mean force on the wall is a monotonically increasing function of the deflector angle $\theta$. However, surprisingly, for sufficiently dilute particle streams our numerical simulations show that increasing $\theta$ may actually cause the force to decrease. Furthermore, for sufficiently localized streams, more complicated phenomena occurs.

In Fig. 3 we plot the mean force in numerical simulations as a function of the deflector angle $\theta$ with different parameters $S$ and $V$ for $e$=$e_w$=0.8. Figure 3(a) shows that when $S$=5, small values of $V$ (e.g., $V$=5) make the mean force increase as the angle $\theta$ increases as one may naively expect. However, for larger values of $V$ (e.g., $V$=10,20,50), increasing $\theta$ can decrease the force experienced by the wall. There exists a critical $\theta$ such that the force reaches its maximum, and further increasing $\theta$ will decrease the force. In Fig. 3(b) we see that a similar phenomena occurs when we choose a smaller value of $S$ (e.g., $S$=1). In this case the nonmonotonic behavior occurs at smaller values of $V$. Figure 3(c) shows a case of a highly localized stream (e.g., $S$=0.1). In this case, for large $V$, the force first increases, then decreases and finally increases again, as $\theta$ increases.

In Fig. 4 we show the results for the mean force as a function of the particle-particle restitution coefficient $e$ for three different angles $\theta$. Figure 4(a) shows that when $\theta$ =84.5°, the mean force experienced by the wall decreases as e increases, while Fig. 4(c) shows just the opposite case for $\theta$=89.5°. Figure 4(b) shows an interesting case for $\theta$=86° in which the force is a nonmonotonic function of $e$. In the next section, we develop a simple theoretical model that gives good quantitative agreement with our numerical results and allows us to isolate the mechanisms responsible for the phenomena mentioned above.

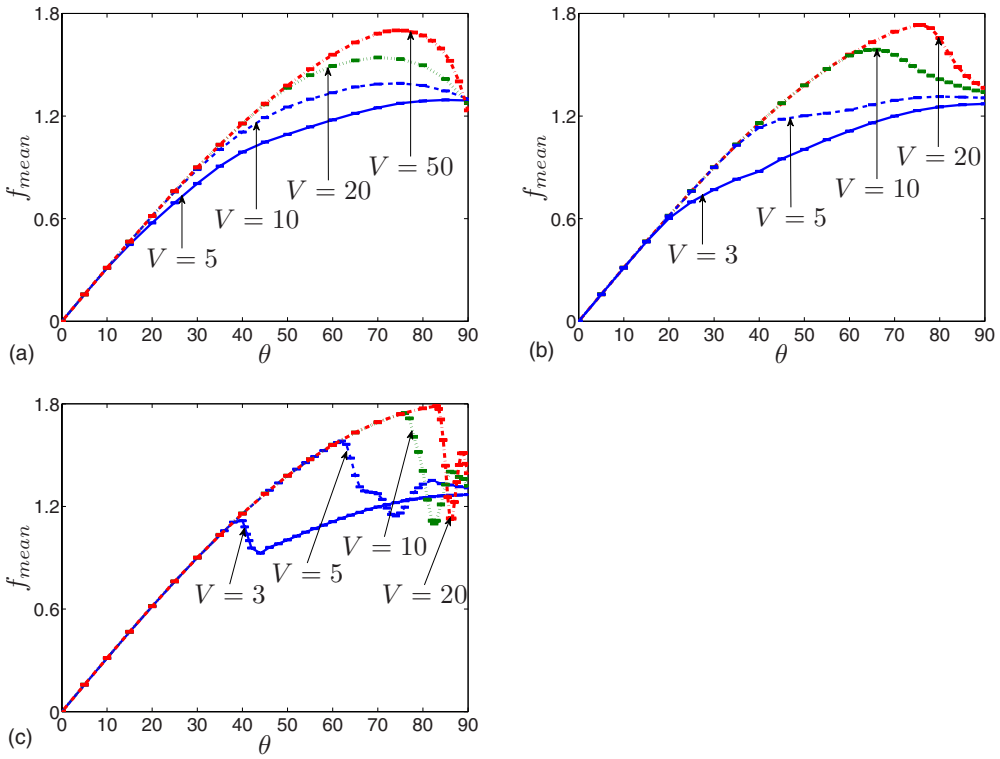


FIG. 3. (Color online) Interesting phenomena of the mean force $f_{mean}$ versus the deflector angle $\theta$ when a statistically steady state has been achieved for (a) $V$=5 (solid blue), $V$=10 (dashed blue), $V$=20 (dotted green) and $V$=50 (dot dashed red) with $S$=5; (b) $V$=3 (solid blue), $V$=5 (dashed blue), $V$=10 (dotted green) and $V$=20 (dot dashed red) with $S$=1; (c) $V$=3 (solid blue), $V$=5 (dashed blue), $V$=10 (dotted green) and $V$=20 (dot dashed red) with $S$=0.1. Other parameters are $e$=$e_w$=0.8. The figure shows that large deflector angle may decrease the force and even increase it again for sufficiently localized particle streams.

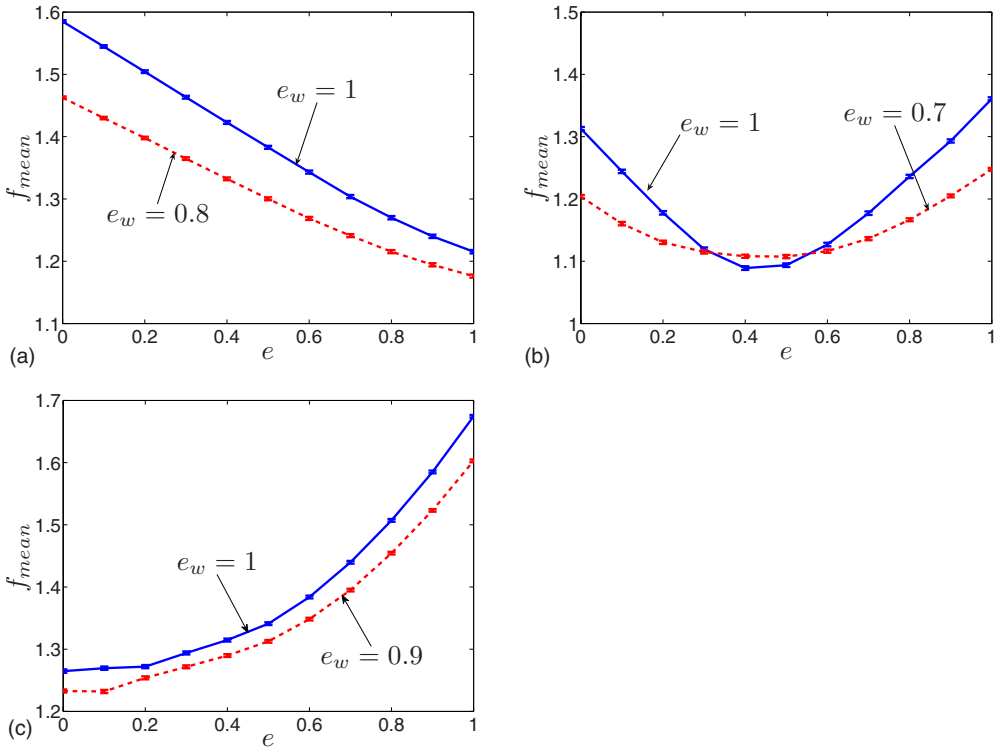


FIG. 4. (Color online) Three cases of the mean force $f_{mean}$ versus the restitution coefficient $e$ in particle-particle collisions when a statistically steady state has been achieved for (a) $e_w$=1 (solid blue) and $e_w$=0.8 (dashed red) with $\theta$=84.5°; (b) $e_w$=1 (solid blue) and $e_w$=0.7 (dashed red) with $\theta$=86°; (c) $e_w$=1 (solid blue) and $e_w$=0.9 (dashed red) with $\theta$=89.5°. The other parameters are $V$=16 and $S$=0.1.

## IV. THEORETICAL APPROACH AND RESULTS

In this section, we aim to investigate the mean force experienced by the oblique wall through a theoretical analysis so that we can interpret the surprising phenomena we have found in our numerical simulations.

We first note that the surprising behavior observed in Figs. 3 and 4 occurs when $V$ is large. This suggests that the particles are highly dilute and so collisions between particles are rare. If the system is very dilute, almost all particles will collide with the wall and propagate to infinity without interacting with any other particle [see Fig. 5(a)]. In this case the dimensionless force $f_{mean}$ can be explicitly computed and is given by $f_{mean}=(1+e_w)\sin\theta$. This is clearly a monotonically increasing function of the angle $\theta$, and it is independent of the restitution coefficient $e$, i.e., $df_{mean}/de=0$. Therefore, the phenomena observed in Sec. III must arise from the effects of particle-particle collisions.

In order to investigate the first effects of collisions between particles, we assume that each particle can only experience one collision with another particle. After this particle-particle collision, one or both of the two particles can hit the wall again, but we will neglect further particle-particle collisions. As we will show in Sec. V, for dilute systems, it is sufficient to consider the case in which only one particle-particle collision can take place for each particle. We will derive an analytical formula for the mean force based on this assumption. For denser systems, more particles experience more than one particle-particle collision. It is extremely difficult to conduct a theoretical analysis that includes multiple particle-particle collisions. However, as we will show, our analysis allows us to explain the qualitative feature of the results from full numerical simulations which contain multiple particle-particle collisions and identify the fundamental mechanisms underlying the behavior.

With this simplification we can determine the total average impulse on the wall by analyzing the possible interactions between any two particles. We denote two adjacent particles as $B_1$ and $B_2$ where $B_1$ is the particle directly ahead of $B_2$.

Because of the randomness in the positions of the two particles in the stream, there are three possible outcomes. The first possibility is that both particles collide with the wall and propagate to infinity with rebound velocity $\vec{\boldsymbol{v}_b}=(\boldsymbol{v_{b1}},\boldsymbol{v_{b2}})^T$ without any particle-particle collision, as shown in Fig. 5(a). The other two possibilities are that $B_2$ can collide with $B_1$ after $B_1$ rebounds from the wall, after which one or both of the particles may hit the wall again only once and propagate to infinity with post-collision velocity $\vec{\boldsymbol{v}_p}=(\boldsymbol{v_{p1}},\boldsymbol{v_{p2}})^T$, as shown in Figs. 5(b) and 5(c).

Next we analyze the probability that a given particle experiences a particle-particle collision, and hence derive an expression for the mean force experienced by the wall. We denote the $n$th particle by $B_n$, and define the following events:

$$C_{n,j}=\{B_n \ collides \ with \ B_j\},$$

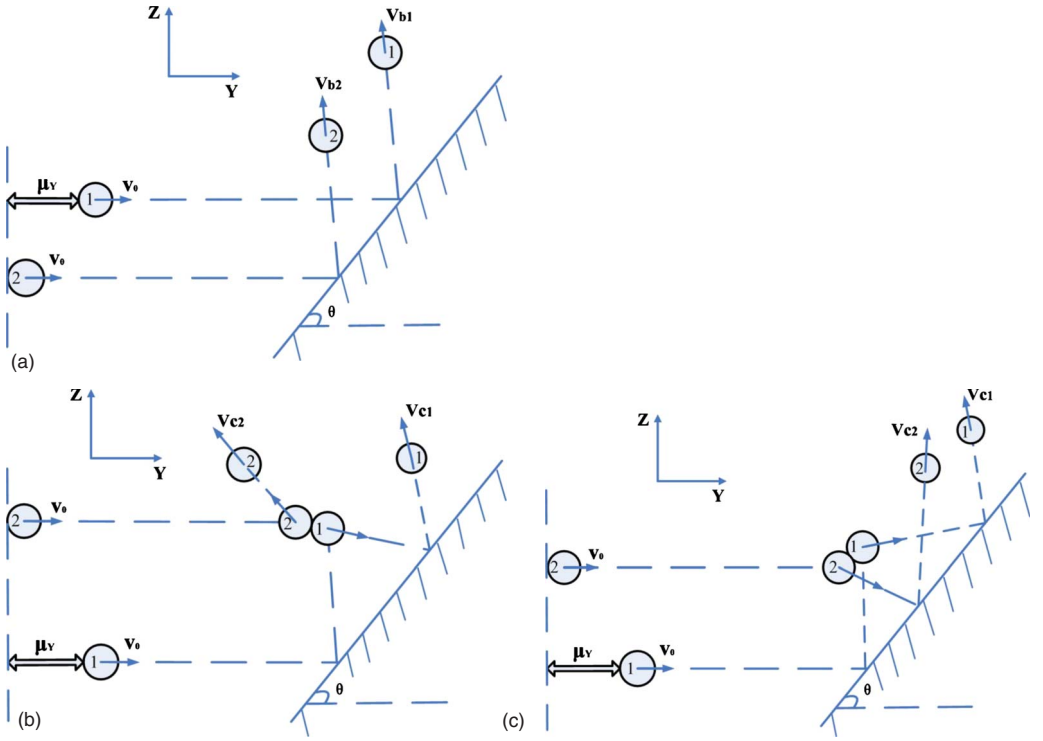


FIG. 5. (Color online) Sketch for the three possible ways in which two particles pass through the system. (a) Both of them can be rebounded by the wall without any particle-particle collision; (b) $B_2$ can collide with $B_1$ after $B_1$ rebounds from the wall, after which one of them hits the wall again; (c) $B_2$ can collide with $B_1$ after $B_1$ rebounds from the wall, after which both of them hits the wall again.

$$D_n = \{B_n \text{ collides with any of the previous particles}\},$$

$$M_n = \{B_n \text{ experiences a collision}\} \quad \text{for all } n, j \in \mathbb{Z}.$$

Then by the above definition, we can write $D_n$ and $M_n$ as

$$D_n = \bigcup_{j=0}^{n-1} C_{n,j}, \quad M_n = \bigcup_{j=0}^{+\infty} C_{n,j}.$$

According to our assumption, $B_n$ may collide with at most one of the particles $\{B_0, B_1, \ldots B_{n-1}, B_{n+1}, B_{n+2} \ldots\}$ before propagating to infinity without experiencing further collisions. That is

$$C_{n,j} \bigcap C_{n,k} = \varnothing \ (\forall j \neq k).$$

First we consider the simple case where $B_n$ may only collide with its nearest neighbors $B_{n-1}$ or $B_{n+1}$. That is, $C_{n,n-j} = \varnothing \ (2 \leq j \leq n, \forall n, j \in \mathbb{Z})$. In this case, we can obtain that the probability of $B_n$ colliding with any of the previous particles is equal to the probability of $B_n$ colliding with $B_{n-1}$. That is

$$\mathbb{P}(D_n) = \mathbb{P}\left(\bigcup_{j=0}^{n-1} C_{n,j}\right) = \mathbb{P}(C_{n,n-1}).$$

We can also obtain that the probability of $B_n$ experiencing a collision equals to the sum of the probability of $B_n$ colliding with $B_{n-1}$ and the probability of $B_n$ colliding with $B_{n+1}$. That is

$$\mathbb{P}(M_n) = \mathbb{P}\left(\bigcup_{j=0}^{+\infty} C_{n,j}\right) = \mathbb{P}(C_{n,n-1}) + \mathbb{P}(C_{n+1,n})$$
$$= \mathbb{P}(D_n) + \mathbb{P}(D_{n+1}).$$

Note that we assume that each particle can experience at most one particle-particle collision and hence $B_n$ may collide with $B_{n-1}$ if and only if $B_{n-1}$ does not collide with the previous particle $B_{n-2}$. Thus we can write the probability of $D_n$ as follows:

$$\mathbb{P}(D_n) = \mathbb{P}(C_{n,n-1}) = \mathbb{P}(C_{n,n-1}|\overline{D_{n-1}}) \cdot \mathbb{P}(\overline{D_{n-1}})$$
$$= \mathbb{P}(C_{n,n-1}|\overline{D_{n-1}}) \cdot [1 - \mathbb{P}(D_{n-1})] \quad (1)$$

where overbar denotes complement. Let $p_1$ denote the probability of a single particle colliding with its previous particles in this case, and $P_1$ denote the probability of a single particle experiencing a collision. When a steady state has been achieved, there will be no difference between the states of $B_n$ and the states of other particles, and hence letting $n \to +\infty$ in Eq. (1), we can obtain $p_1$ and $P_1$ as

$$p_1 = \lim_{n \to +\infty} \mathbb{P}(D_n) = \frac{p_\tau}{1 + p_\tau}, \quad (2)$$

$$P_1 = \lim_{n \to +\infty} \mathbb{P}(M_n) = \lim_{n \to +\infty} \mathbb{P}(D_n) + \lim_{n \to +\infty} \mathbb{P}(D_{n+1})$$
$$= 2 \lim_{n \to +\infty} \mathbb{P}(D_n) = 2p_1 = \frac{2p_\tau}{1 + p_\tau} \quad (3)$$

where

$$p_\tau = \mathbb{P}(C_{n,n-1}|\overline{D_{n-1}}) \quad \forall\, n \in \mathbb{Z} \tag{4}$$

denotes the probability of a single particle experiencing a particle-particle collision with its previous nearest particle subject to the condition that the previous neighboring particle does not collide with its previous particle.

The force experienced by the oblique wall, denoted by $F$, consists of two components. One, denoted by $F_w$, is the impact caused by the direct particle-wall collision without any collision with previous particles. The other, denoted by $F_{cw}$, is the impact caused by the particle-wall collision after the particle-particle collision. For example, $B_n$ can directly hit the wall before experiencing a possible particle-particle collision if and only if it does not collide with the previous particle $B_{n-1}$, or $B_n$ can hit the wall after the particle-particle collision with $B_{n-1}$ only if $B_{n-1}$ does not hit its previous particle $B_{n-2}$. Therefore we can write the total average impulse on the wall as

$$\begin{aligned}\mathbb{E}(F) &= \mathbb{E}(F_w) + \mathbb{E}(F_{cw}) \\ &= \mathbb{E}(F_w|\overline{D_n}) \cdot \mathbb{P}(\overline{D_n}) + \mathbb{E}(F_{cw}|\overline{D_{n-1}}) \cdot \mathbb{P}(\overline{D_{n-1}}) \\ &= \mathbb{E}(F_w|\overline{D_n}) \cdot (1 - \mathbb{P}(D_n)) + \mathbb{E}(F_{cw}|\overline{D_{n-1}}) \cdot (1 - \mathbb{P}(D_{n-1})).\end{aligned}$$

For a steady state and $n \to +\infty$, we obtain,

$$\begin{aligned}F_{mean}^{(1)} &= (1 - p_1)[\lim_{n\to+\infty} \mathbb{E}(F_w|\overline{D_n}) + \lim_{n\to+\infty} \mathbb{E}(F_{cw}|\overline{D_{n-1}})] \\ &= \frac{1}{1 + p_\tau}(\tilde{F}_w + \tilde{F}_{cw})\end{aligned} \tag{5}$$

where $F_{mean}^{(1)}$ denotes the average force experienced by the oblique wall when we only include the effect of the nearest neighbors, $\tilde{F}_w$ denotes the average impact on the wall caused by a single particle to which the first collision is with the wall, and $\tilde{F}_{cw}$ denotes the average impact on the wall after the particle collides with the previous neighbor when the neighboring particle itself does not experience a collision with its previous neighbor.

Now let us consider the more complicated case where $B_n$ may also collide with the next nearest neighboring particles. That is $B_n$ may collide with two previous particles $B_{n-1}$ and $B_{n-2}$ or two later particles $B_{n+1}$ and $B_{n+2}$, i.e $C_{n,n-j} = \emptyset$ $(3 \le j \le n, \forall\, n, j \in \mathbb{Z})$. In this case, we can write the probability of $B_n$ colliding with any of the previous particles as the sum of the probability of $B_n$ colliding with $B_{n-1}$ and the probability of $B_n$ colliding with $B_{n-2}$. That is

$$\begin{aligned}\mathbb{P}(D_n) &= \mathbb{P}\left(\bigcup_{j=0}^{n-1} C_{n,j}\right) = \mathbb{P}\left(C_{n,n-1} \bigcup C_{n,n-2}\right) \\ &= \mathbb{P}(C_{n,n-1}) + \mathbb{P}(C_{n,n-2}).\end{aligned}$$

We can also write the probability of $B_n$ experiencing a collision as the sum of following probabilities:

$$\begin{aligned}\mathbb{P}(M_n) &= \mathbb{P}\left(\bigcup_{j=0}^{+\infty} C_{n,j}\right) = \mathbb{P}(C_{n,n-1}) + \mathbb{P}(C_{n,n-2}) + \mathbb{P}(C_{n+1,n}) \\ &\quad + \mathbb{P}(C_{n+2,n}).\end{aligned}$$

Following a similar approach in deriving Eqs. (2) and (3), when a steady state has been achieved, we obtain,

$$\lim_{n\to+\infty} \mathbb{P}(C_{n,n-1}) = \lim_{n\to+\infty} \mathbb{P}(\overline{D_{n-1}}) \cdot \frac{p_\tau(1 - p_\pi p_{2\tau})}{1 - p_\pi p_{2\tau} + (1 - p_\tau)^2 p_{2\tau}}, \tag{6}$$

$$\lim_{n\to+\infty} \mathbb{P}(C_{n,n-2}) = \lim_{n\to+\infty} \mathbb{P}(\overline{D_{n-2}}) \cdot \frac{p_{2\tau}(1 - p_\tau)^2(1 + p_{2\tau})}{1 - p_\pi p_{2\tau} + (1 - p_\tau)^2 p_{2\tau}} \tag{7}$$

where $p_\tau$ is defined in Eq. (4), and

$$p_{2\tau} = \mathbb{P}\left(C_{n,n-2}|\overline{C_{n,n-1}} \bigcap \overline{C_{n-1,n-2}} \bigcap \overline{D_{n-2}}\right) \quad \forall\, n \in \mathbb{Z} \tag{8}$$

is the probability of a single particle experiencing a particle-particle collision with its next previous particle subject to the condition that the nearest previous neighboring particle does not collide with its nearest previous and later particles and the next previous particle does not collide with its previous particles.

Let $p_2$ denote the probability of a single particle colliding with previous particles in this case, and $P_2$ denote the probability of a single particle experiencing a collision, thus we can write $p_2$ and $P_2$ as

$$\begin{aligned}p_2 &= \lim_{n\to+\infty} \mathbb{P}(D_n) = \lim_{n\to+\infty} \mathbb{P}(C_{n,n-1}) + \lim_{n\to+\infty} \mathbb{P}(C_{n,n-2}) \\ &= \frac{p_\tau + B}{1 + p_\tau + B},\end{aligned} \tag{9}$$

$$\begin{aligned}P_2 &= \lim_{n\to+\infty} \mathbb{P}(M_n) = 2 \lim_{n\to+\infty} \mathbb{P}(C_{n,n-1}) + 2 \lim_{n\to+\infty} \mathbb{P}(C_{n,n-2}) \\ &= 2 \lim_{n\to+\infty} \mathbb{P}(D_n) = 2p_2 = \frac{2(p_\tau + B)}{1 + p_\tau + B}\end{aligned} \tag{10}$$

where

$$B = \frac{p_{2\tau}(1 - p_\tau)^2(1 - p_\tau + p_{2\tau})}{1 - p_\pi p_{2\tau} + (1 - p_\tau)^2 p_{2\tau}}. \tag{11}$$

In this case, the force experienced by the oblique wall consists of three components. One is $F_w$ which is the impact caused by the direct particle-wall collision without any collision with previous particles. The other two, denoted by $F_{cw1}$ and $F_{cw2}$, are the impacts which are caused by particle-wall collisions after particle-particle collisions with its previous two neighbors. For example, $B_n$ can directly hit the wall if and only if it does not collide with previous two particles $B_{n-1}$ and $B_{n-2}$, otherwise it may hit the wall after colliding with either $B_{n-1}$ or $B_{n-2}$. Therefore, by an analysis similar to the previous case we can write the total average impact on the wall as follows:

$$\mathbb{E}(F) = \mathbb{E}(F_w) + \mathbb{E}(F_{cw1}) + \mathbb{E}(F_{cw2}) = \mathbb{E}(F_w|\overline{D_n}) \cdot \mathbb{P}(\overline{D_n}) + \mathbb{E}\left(F_{cw1}|\overline{C_{n,n-2}} \bigcap \overline{D_{n-1}}\right) \cdot \mathbb{P}(\overline{C_{n,n-2}} \bigcap \overline{D_{n-1}}) + \mathbb{E}(F_{cw2}|\overline{C_{n,n-1}} \bigcap \overline{C_{n-1,n-2}} \bigcap \overline{D_{n-2}}) \times \mathbb{P}\left(\overline{C_{n,n-1}} \bigcap \overline{C_{n-1,n-2}} \bigcap \overline{D_{n-2}}\right). \quad (12)$$

To obtain the force when a steady state has been achieved, we let $n \to +\infty$ and after some algebra and the use of elementary probability, we obtain,

$$F_{mean}^{(2)} = \frac{1}{1+p_\tau+B}\left[\widetilde{F}_w + \frac{1-p_\pi p_{2\tau}}{1-p_\pi p_{2\tau}+(1-p_\tau)^2 p_{2\tau}}\widetilde{F}_{cw1} + \frac{(1-p_\tau)^2(1+p_{2\tau})}{1-p_\pi p_{2\tau}+(1-p_\tau)^2 p_{2\tau}}\widetilde{F}_{cw2}\right], \quad (13)$$

where $F_{mean}^{(2)}$ denotes the average force experienced by the oblique wall when the interactions with the nearest and the next nearest neighbors are both included, and $B$ is defined in Eq. (11). The quantity $\widetilde{F}_w = \lim_{n\to+\infty} \mathbb{E}(F_w|\overline{D_n})$ denotes the average impact on the wall caused by directly hitting the wall when a single particle does not collide with previous ones. The quantity $\widetilde{F}_{cw1} = \lim_{n\to+\infty} \mathbb{E}(F_{cw1}|\overline{C_{n,n-2}} \cap \overline{D_{n-1}})$ denotes the average impact on the wall caused by the particle-wall collision after the particle-particle collision between $B_n$ and $B_{n-1}$, and $\widetilde{F}_{cw2} = \lim_{n\to+\infty} \mathbb{E}(F_{cw2}|\overline{C_{n,n-1}} \cap \overline{C_{n-1,n-2}} \cap \overline{D_{n-2}})$ denotes the counterpart of $\widetilde{F}_{cw1}$ after the particle-particle collision between $B_n$ and $B_{n-2}$.

In principle, we can follow this procedure to include more particle-particle collisions in calculating the mean force. By comparing Eqs. (2) and (9) we see that the effect of including collisions with the next nearest neighbors is the replacing $p_\tau$ by $p_\tau + B$ where $B$ is relatively small to $p_\tau$ for a dilute system. For simplicity we choose $p_1 = \frac{p_\tau}{1+p_\tau}$ as the approximate probability for a single particle to collide with previous particles in the system, and use Eq. (5) to evaluate the mean force experienced by the wall. In Sec. VI, we will show that including interactions with more previous particles does not qualitatively affect the phenomena we present here, and the correction is indeed small for a dilute system.

According to the formula (5), we can determine $\widetilde{F}_w$ and $\widetilde{F}_{cw}$ by analyzing pairwise particle-particle collisions, and thus to determine $F_{mean}$. We still denote the two particles $B_1$ and $B_2$ where $B_1$ is the particle that immediately precedes the particle $B_2$. Let $z_1$ and $z_2$, respectively, denote their initial heights which are independent random variables. Because of the randomness of $z_1$ and $z_2$, the rebound velocity $\vec{\boldsymbol{v}_b}$ and the postcollision velocity $\vec{\boldsymbol{v}_p}$ are random variables related to $z_1$ and $z_2$. Notice that the impact on the wall depends on $\vec{\boldsymbol{v}_b}$ and $\vec{\boldsymbol{v}_p}$, and consequently on $z_1$ and $z_2$, thus we can write the mean force $F_{mean}$ as follows:

$$F_{mean} = \frac{1}{1+p_\tau}(\widetilde{F}_w + \widetilde{F}_{cw}), \quad (14)$$

where

$$\widetilde{F}_w = F_b[\boldsymbol{v_b}(z_1,z_2)], \quad (15)$$

$$\widetilde{F}_{cw} = \mathbb{E}(F_p \cdot \mathbf{1}_A) = \int\int_A F_p[\boldsymbol{v_p}(z_1,z_2)]\rho(z_1,z_2)dz_1dz_2. \quad (16)$$

Here $F_b$ and $F_p$ denote the impact on the wall caused by the rebound velocity $\vec{\boldsymbol{v}_b}$ and the postcollision velocity $\vec{\boldsymbol{v}_p}$, respectively, and $\rho(z_1,z_2)$ is the joint distribution density of $z_1$ and $z_2$. The quantity $\mathbf{1}_A(z_1,z_2)$ denotes the indicator function of the set $A$, i.e.,

$$\mathbf{1}_A(z_1,z_2) = \begin{cases} 1 & \text{if } (z_1,z_2) \in A \\ 0 & \text{otherwise} \end{cases},$$

where

$$A = \{(z_1,z_2) \in \mathbb{R}^2 | C_{2,1}\}.$$

Using Eq. (14), a straightforward calculation (see Appendix A), gives the analytical formula for the dimensionless mean force $f_{mean}$ as

$$f_{mean} = \frac{(1+e_w)\sin\theta}{4+2\ \mathrm{erf}(C_-)-4\ \mathrm{erf}(C_+)} \cdot \left\{ 4 + ((1+e)-e_w(1-e))(\mathrm{erf}(D_-)-\mathrm{erf}(D_+)) + ((1-e)-e_w(1+e)) \times \left[ \mathrm{erf}(C_-)-\mathrm{erf}(C_+) + \mathrm{H}\left(e_w - \frac{1-e}{1+e}\right)(\mathrm{erf}(K_+)-\mathrm{erf}(K_-)) \right] + (1+e)(1+e_w) \times \left[ \left(\frac{S^2\sin^2\theta}{2} + \frac{V^2\cos^2\theta}{4}\right)\left(\mathrm{erf}(C_-)-\mathrm{erf}(C_+)+\mathrm{erf}(D_+)-\mathrm{erf}(D_-)+\mathrm{H}\left(e_w-\frac{1-e}{1+e}\right)(\mathrm{erf}(K_+)-\mathrm{erf}(K_-))\right) + \frac{VS\sin\theta\cos\theta}{\sqrt{\pi}} \cdot \left(e^{-C_+^2} - e^{-C_-^2} + e^{-D_-^2} - e^{-D_+^2} + \mathrm{H}\left(e_w - \frac{1-e}{1+e}\right)(e^{-K_-^2} - e^{-K_+^2})\right) + \frac{S^2\sin^2\theta}{\sqrt{\pi}}\left(C_+e^{-C_+^2} - C_-e^{-C_-^2} + D_-e^{-D_-^2} - D_+e^{-D_+^2} + \mathrm{H}\left(e_w - \frac{1-e}{1+e}\right)(K_-e^{-K_-^2} - K_+e^{-K_+^2})\right) \right] \right\}, \quad (17)$$

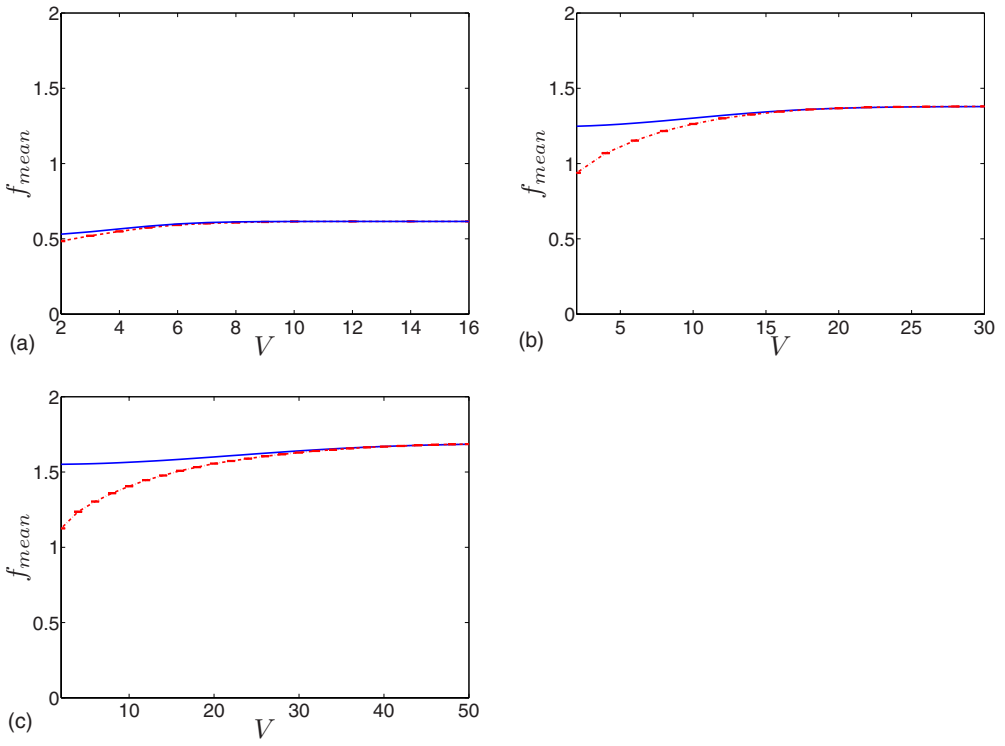


FIG. 6. (Color online) Comparison between theoretical results (solid blue) and numerical results (dashed red) for the mean force $f_{mean}$ against the parameter $V$ for (a) $\theta=20°$; (b) $\theta=50°$; (c) $\theta=70°$. The other parameters are $S=5$ and $e=e_w=0.8$. Our theoretical results match the numerical results when $V\cos\theta \gg 1$, and for larger values of $\theta$, one requires larger values of $V$ for our approximation to be good.

where

$$\mathrm{erf}(x)=\frac{2}{\sqrt{\pi}}\int_0^x e^{-t^2}dt, \quad \mathrm{H}(x)=\begin{cases}1 & \text{if } x\geq 0\\ 0 & \text{if } x<0\end{cases}$$

are Error function and Heaviside function, respectively, and

$$C_{\pm}=\frac{\mp 1-\dfrac{V\cos\theta}{2}}{S\sin\theta},$$

$$D_{\pm}=\frac{\mp\sqrt{\dfrac{(1+e)-e_w(1-e)}{(1+e)(1+e_w)}}-\dfrac{V\cos\theta}{2}}{S\sin\theta},$$

$$K_{\pm}=\frac{\mp\sqrt{\dfrac{e_w(1+e)-(1-e)}{(1+e)(1+e_w)}}-\dfrac{V\cos\theta}{2}}{S\sin\theta}.$$

The methodology in a two-dimensional system can be extended to three-dimensions in a straightforward way. The main difference is that there will be another distribution representing the initial location in the third dimension. This will lead to an extra collision angle similar to $\varphi$ (see Fig. 23 in Appendix A) when two particles collide with each other. For theoretical analysis, this implies that in three dimensions we need to perform one more integral to obtain the analytical formula for the mean force.

We note that, Eq. (17) was derived under the assumption that the distribution of the distance between particles in the $Y$ direction, $\rho_Y$, is nonrandom. If we relax this assumption, then the quantity $V$ in Eq. (17) can be interpreted as a random variable and it is easy to show that the mean force is the expected value of Eq. (17) with respect to the probability density of $V$.

## V. VALIDITY

In this section we will derive conditions under which our theoretical prediction for the mean force given by Eq. (17) will be valid. In our theoretical derivation, we assumed that each particle could experience at most one particle-particle collision. Therefore, our theory should give a good approximation when the fraction of particles that experience at least two particle-particle collisions is low. In Appendix B 1, we show that if $V\cos\theta \gg 1$, then the probability of a particle experiencing a particle-particle collision is low. In this case the probability of a particle experiencing at least two particle-particle collisions must also be low, and so our theory will be valid. In Fig. 6, we plot the theoretical results for the mean force $f_{mean}$ (solid blue line) together with the numerical results (dashed red line) as functions of the parameter $V$ with different deflector angles for $S=5$. From the figures, we see that our theoretical results match the numerical results when $V\cos\theta \gg 1$. The figures also show that for larger values of $\theta$, one requires larger values of $V$ for our approximation to be good.

However, when the deflector angle $\theta$ is close to $\frac{\pi}{2}$, the particles in the stream have high probabilities to experience

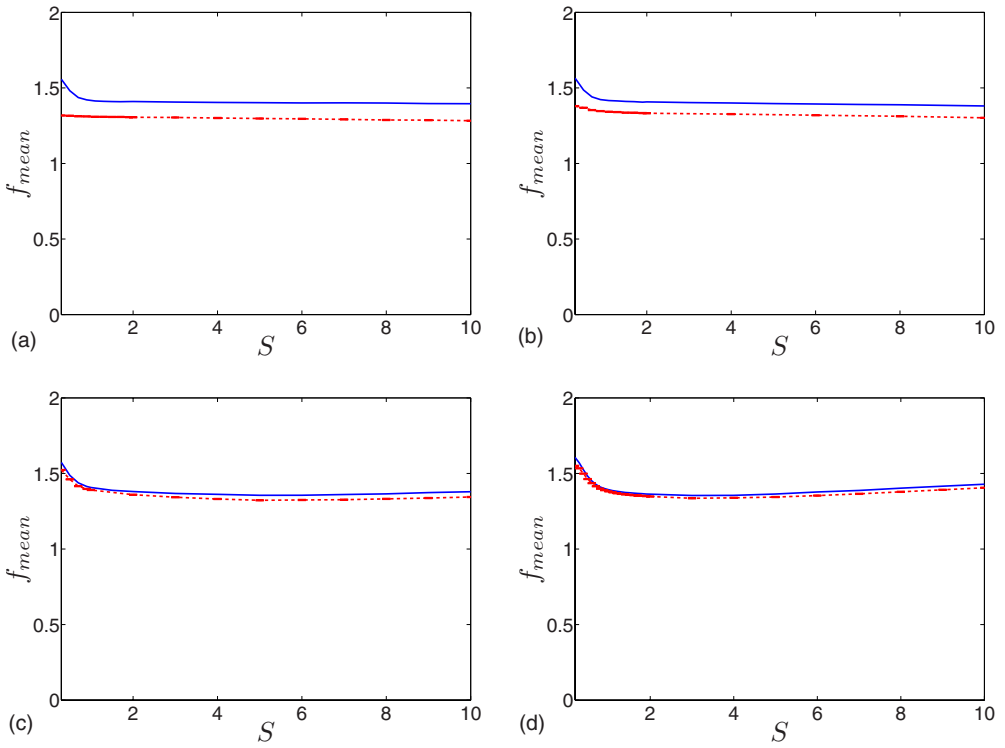


FIG. 7. (Color online) Comparison between theoretical results (solid blue) and numerical results (dashed red) for the mean force $f_{mean}$ against the parameter $S$ for (a) $V=5$; (b) $V=10$; (c) $V=50$; (d) $V=75$; The other parameters are $\theta=90°$ and $e=e_w=0.8$. For larger values of $V$, our theoretical and numerical results agree more closely over a wider range of $S$ values.

their first particle-particle collision. In this case, the condition $V\cos\theta \gg 1$ is not the appropriate condition for the validity of our theory. In Appendix B 2, we show that if $V \gg 1$ and $V \gg S$, the probability of particles experiencing two particle-particle collisions is also low, and so our theory will be valid if $V \gg 1$ and $V \gg S$. In this case, the probability of a particle experiencing a particle-particle collision is not necessarily low. That is, our theory can also work if the probability of a particle experiencing a particle-particle collision is high as long as the probability of particles experiencing two particle-particle collisions is low, which implies most particles in the system experience either zero or a single particle-particle collision. In Fig. 7, we plot the theoretical results for the mean force $f_{mean}$ (solid blue line) together with the numerical results (dashed red line) as functions of the parameter $S$ with different values of $V$ for $\theta=90°$. From the figures, we see that for larger values of $V$, our theoretical and numerical results agree more closely over a wider range of $S$ values. This means that the larger the value of $V$, the wider the particle stream can be before our theoretical prediction will break down.

In the subfigures in the left column of Figs. 8–11, we plot the theoretical results for the mean force (solid red lines), compared with our numerical results (dashed blue lines). In the subfigures in the right column we show the theoretical results for particle-particle collision probability $P_1$ (solid red lines) defined in Eq. (3), in comparison with the results from numerical simulations (dashed blue lines). We also plot the probability of particles experiencing at least two collisions in the numerical simulations (blue circles). These figures show that our theoretical predictions are in good agreement with the numerical results when the probability of particles experiencing at least two collisions is less than about 5%. They also show that the theoretical particle-particle collision probability $P_1$ is lower than the results observed in our simulations. This is due to the assumption that each particle can experience at most one particle-particle collision in our theoretical derivation. However, in our simulations there may be additional collisions neglected by our theory. In the next section, we will explain why taking into account more particle-particle collisions generally makes the mean force experienced by the wall smaller.

From Figs. 8–11, we see that our theory works extremely well for all of the cases in which $V\cos\theta \gg 1$. In Fig. 8, although for large deflector angles the particle-particle collision probability increases rapidly and even approaches 1, the probability of particles experiencing at least two particle-particle collisions can achieve low values. Our theory works very well for this region because the particles only collide with their nearest neighbors and the interactions occur in pairs. Figures 9(a), 11(a), and 11(b) also show that our theory works well for low probability of particles experiencing at least two particle-particle collisions. Although our theory cannot perfectly match the numerical results when the probability of particles experiencing at least two particle-particle collisions is high, see Figs. 9(b), 10, and 11(c), we can still use the theory to give reasonable qualitative analysis for the mean force.

## VI. DISCUSSION

In this section, we show that our theoretical results for the mean force given in Eq. (17) can explain the phenomena

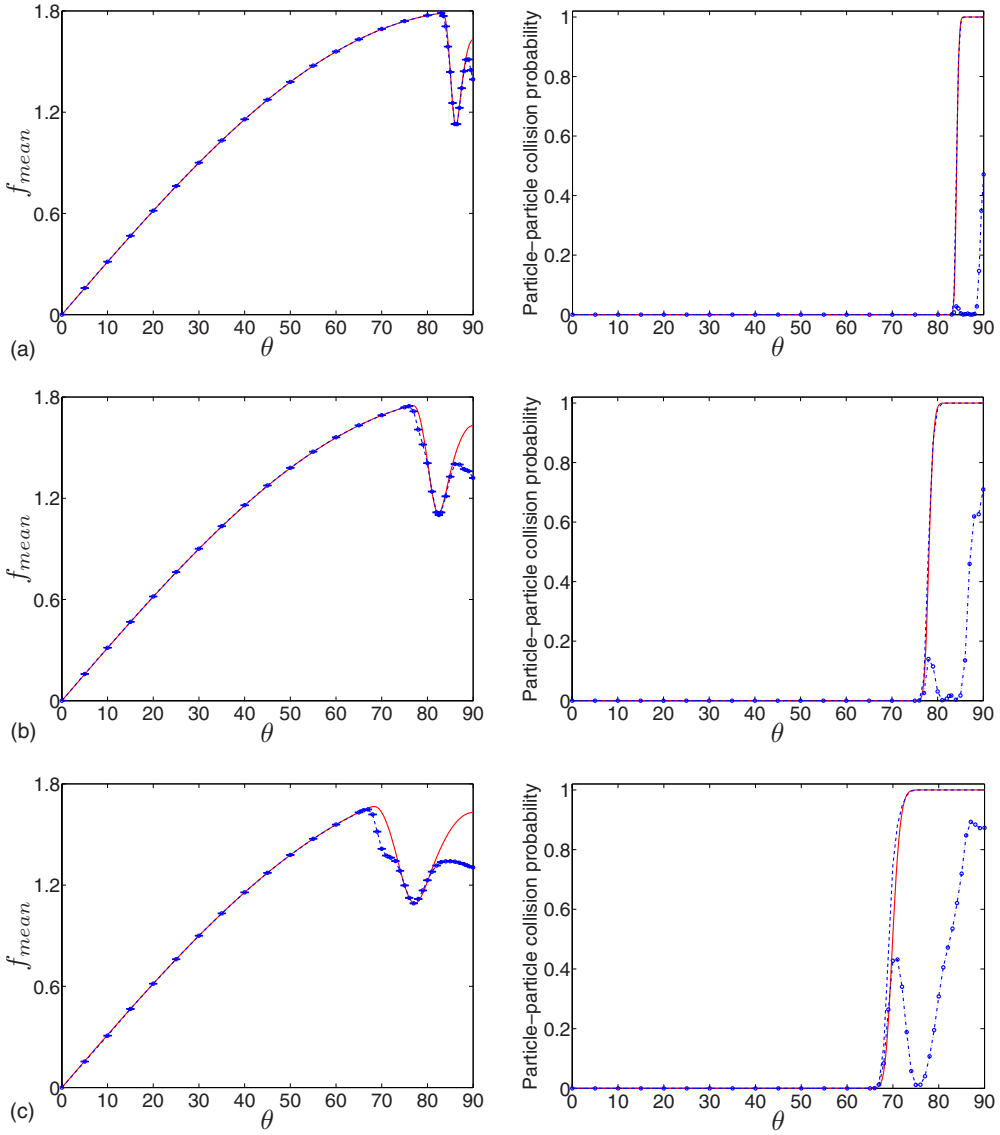


FIG. 8. (Color online) Comparison between theoretical results (solid red) and numerical results (dashed blue) for the mean force $f_{mean}$ against the deflector angle $\theta$, together with corresponding theoretical particle-particle collision probability $P_1$ (solid red), numerical particle-particle collision probability (dashed blue) and the numerical probability of particles that experience at least two particle-particle collisions (blue circle) for (a) $V=20$; (b) $V=10$; (c) $V=6$. The other parameters are $S=0.1$ and $e=e_w=0.8$. In the right-hand side panels of (a) and (b) the solid red curves and the dashed blue curves almost exactly coincide.

found in numerical simulations. For simplicity, we will focus on the case in which the restitution coefficient for particle-wall collisions is unity. Nevertheless, the situations with $e_w<1$ have similar results.

When the particle-wall restitution coefficient is unity ($e_w=1$), we can obtain

$$u_{p1} = v_0 \sin\theta[e-(1+e)q^2], \tag{18}$$

$$u_{p2} = -v_0 \sin\theta[e-(1+e)q^2], \tag{19}$$

where $u_{p1}$ and $u_{p2}$ denote the postcollision velocity components of the two particles in the direction perpendicular to the wall, and $q=\frac{1}{2a}[\mu_Y \cos\theta-(z_2-z_1)\sin\theta]$ (see Appendix A). Thus, after their first particle-particle collision the two particles share the same value of the velocity component perpendicular to the wall, but with opposite directions. Then, the particle approaching the wall (the one with positive velocity component) will experience a collision with the wall that changes the sign of its velocity. Therefore the velocity components perpendicular to the wall are the same after the two particles interact with themselves and the wall. Hence combining Eqs. (A9)–(A12) (see Appendix A), we can write the analytical expression for the mean force $f_{mean}$ in this case as follows:

$$f_{mean} = f_g f_s, \tag{20}$$

where

$$f_g = 2\sin\theta, \tag{21}$$

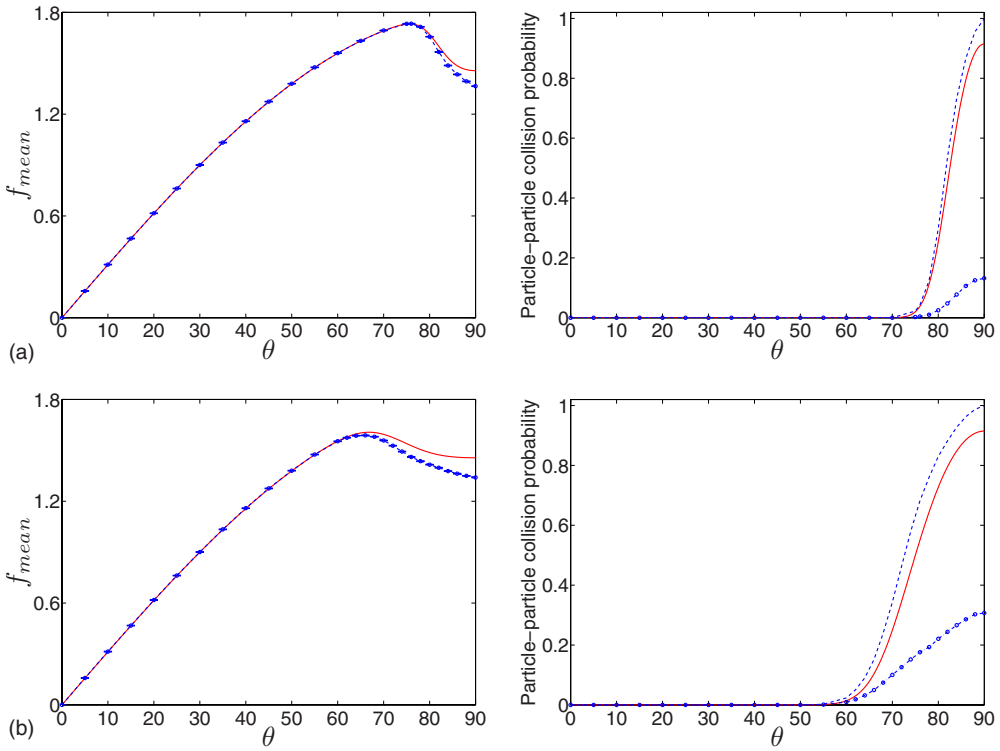


FIG. 9. (Color online) Comparison between theoretical results (solid red) and numerical results (dashed blue) for the mean force $f_{mean}$ against the deflector angle $\theta$, together with corresponding theoretical particle-particle collision probability $P_1$ (solid red), numerical particle-particle collision probability (dashed blue) and the numerical probability of particles that experience at least two particle-particle collisions (blue circle) for (a) $V=20$; (b) $V=10$. The other parameters are $S=1$ and $e=e_w=0.8$.

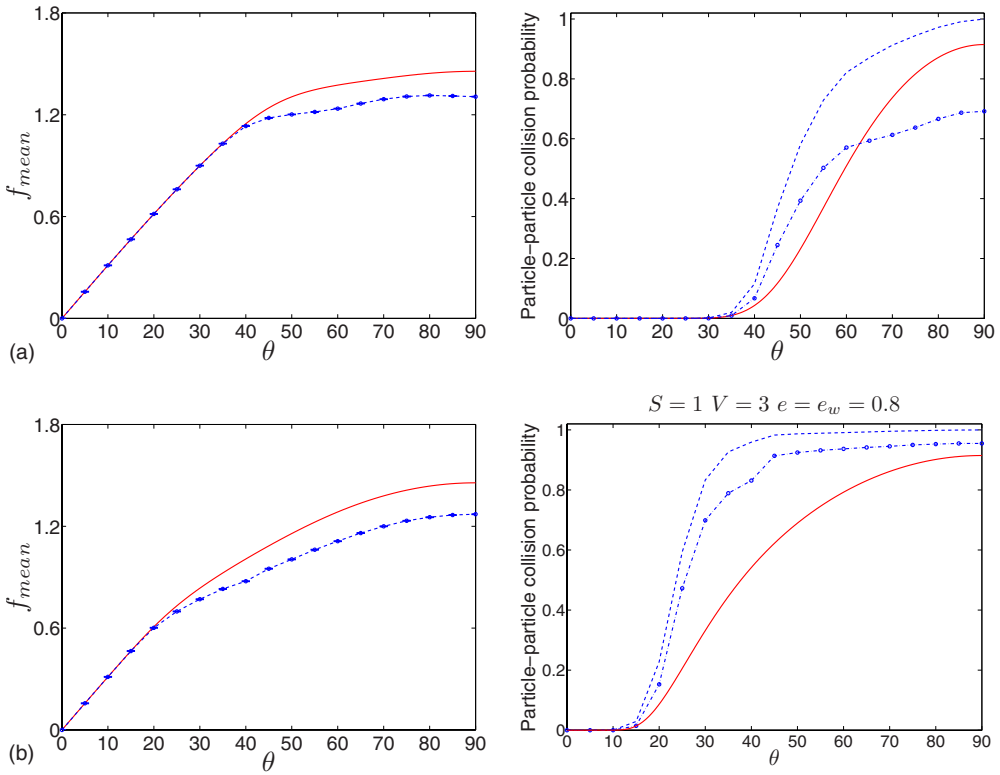


FIG. 10. (Color online) Comparison between theoretical results (solid red) and numerical results (dashed blue) for the mean force $f_{mean}$ against the deflector angle $\theta$, together with corresponding theoretical particle-particle collision probability $P_1$ (solid red), numerical particle-particle collision probability (dashed blue) and the numerical probability of particles that experience at least two particle-particle collisions (blue circle) for (a) $S=1$ and $V=5$; (b) $S=1$ and $V=3$; The other parameters are $e=e_w=0.8$.

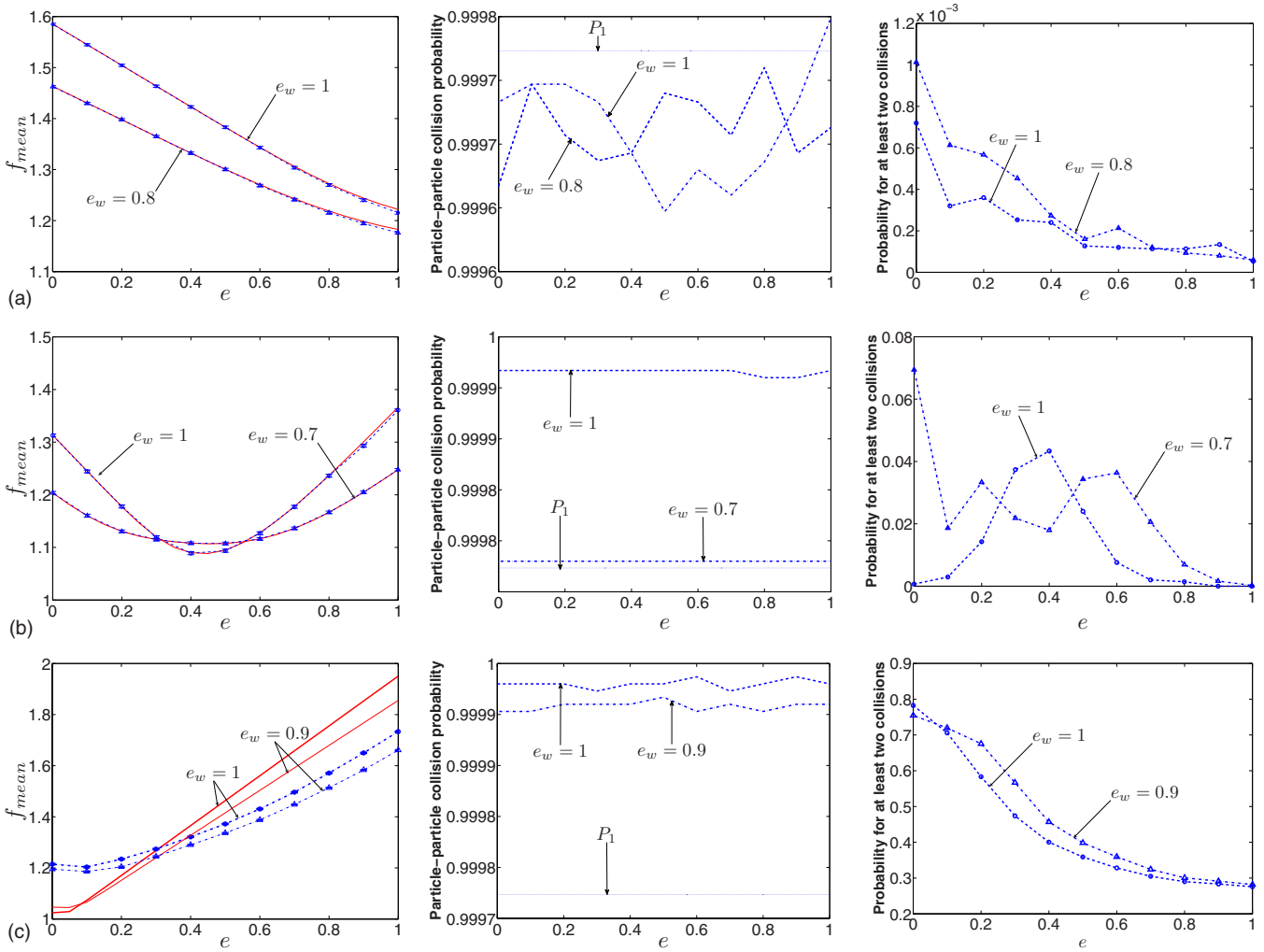


FIG. 11. (Color online) Comparison between theoretical results (solid red) and numerical results (dashed blue) for the mean force $f_{mean}$ against the restitution coefficient $e$, together with corresponding theoretical particle-particle collision probability $P_1$ (solid blue), numerical particle-particle collision probability (dashed blue) and the numerical probability of particles that experience at least two particle-particle collisions (blue circle and blue triangle) for (a) $e_w$=1 and $e_w$=0.8 with $\theta$=84.5°; (b) $e_w$=1 and $e_w$=0.7 with $\theta$=86°; (c) $e_w$=1 and $e_w$=0.9 with $\theta$=89°. The other parameters are $V$=16 and $S$=0.1. In the left-hand side of (a) and (b) the solid red curves and the dashed blue curves almost exactly coincide.

$$f_s = \frac{1 + \int_\Omega |e - (1+e)q^2| \rho(\xi) d\xi}{1 + \int_\Omega \rho(\xi) d\xi}. \tag{22}$$

$\Omega$ and $\rho(\xi)$ are given by Eqs. (A14) and (A15), respectively, (see Appendix A).

In the left column of Fig. 12, we plot the theoretical mean force $f_{mean}$ (solid line) together with $f_g$ (dashed line) as functions of the deflector angle $\theta$. There are three cases similar to the phenomena we have found in numerical simulations. Figure 12(a) shows a monotonically increasing case which is consistent with intuition. Namely, larger angle $\theta$ implies a larger velocity component perpendicular to the wall, and hence larger impulse. We refer to this as a geometric effect, and we quantify it by $f_g$ defined in Eq. (21). Clearly increasing $\theta$ makes the geometric effect stronger, and thus makes the force experienced by the wall increase. However, this effect does not always dominate. Figure 12(b) shows a case in which the mean force increases, reaches a maximum, and then decreases as $\theta$ increases. Figure 12(c) shows the case in which an additional local minimum occurs.

Below we explain the origin of these phenomena. Comparing the curves for $f_{mean}$ and $f_g$ in Fig. 12, it is clear that there exists another effect that decreases the mean force and hence, works against the geometric effect. Since particle-particle collisions do not change the total momentum of the two particles, the impulse experienced by the wall is the net change of momentum experienced by the particles. The wall only exerts a force in the direction perpendicular to the wall. In comparing the three possible outcomes mentioned in Sec. IV, it shows that when particles rebound from the wall they can collide with incoming ones and be scattered. This scattering may reduce the net impulse on the wall. We refer to this effect as shielding.

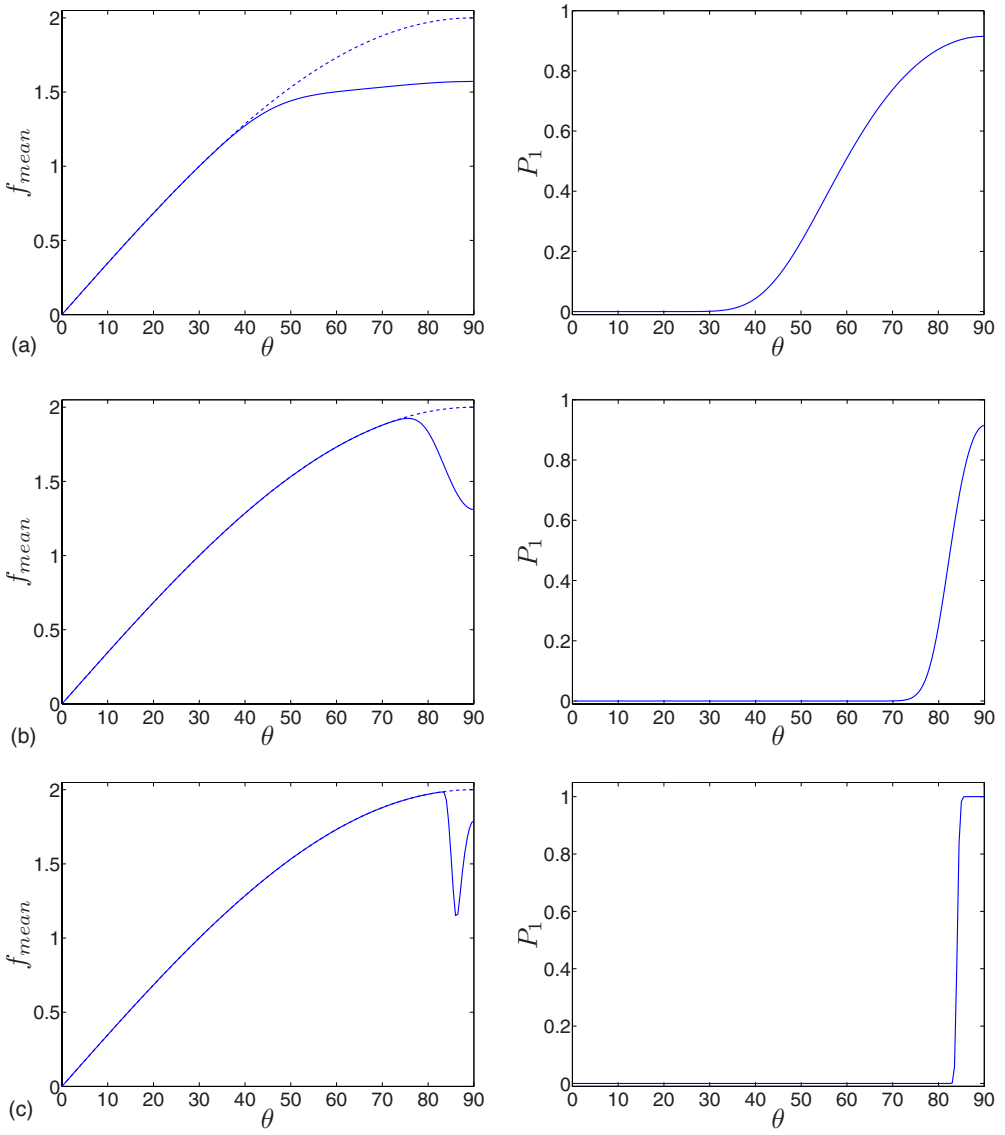


FIG. 12. (Color online) Three cases of the mean force $f_{mean}$ changing against $\theta$ according to our theoretical results (solid) and theoretical geometric effect $f_g$ (dashed), together with corresponding particle-particle collision probability $P_1$ for (a) $V=5$, $S=1$, $e=0.8$; (b) $V=20$, $S=1$, $e=0.2$, and (c) $V=20$, $S=0.1$, $e=0.8$ with $e_w=1$.

The simplest example of shielding is shown in Fig. 13 where we let $\theta=\pi/2$ and the particle-wall restitution coefficient $e_w=1$. The two particles have initial velocity $v_0$. Figure 13(a) shows the case where there is no particle-particle collision. In this case, the two particles are directly rebounded from the wall, and the net impulse is $4v_0$. Figure 13(b) shows the case where the particle $B_2$ collides with $B_1$, and after the collision, they both propagate to the direction parallel to the wall, and the momentum in the direction perpendicular to the wall is zero. Thus the net impulse in this case is $2v_0$ which is smaller than the first case, and thus the force experienced by the wall is smaller. Although in general the particles will scatter to all the possible directions rather than the direction parallel to the wall, it is this kind of scattering after the particle-particle collisions that reduces the net impulse, and thus reduces the force.

We can measure the degree of this shielding effect by $1/f_s$ with $f_s$ given by Eq. (22). Increasing the angle $\theta$ makes the shielding effect become stronger because the larger $\theta$ is, the more likely particles are to collide with each other, thus the increase in the numerator of $1/f_s$ exceeds the increase in the denominator due to $|e-(1+e)q^2| \leq 1$. In the right column of Fig. 12, we plot the theoretical prediction for the particle-particle collision probability $P_1$, defined by Eq. (3), against $\theta$. The figures also show that the probability of a particle-particle collision $P_1$ is a monotonic function of $\theta$.

From the figures of $P_1$ versus $\theta$ in Fig. 12 we know that for small $\theta$, there is a very low probability of particle-particle collisions and thus the shielding effect is weak and the changes in the mean force are dominated by the geometric effect. However, for sufficiently large $\theta$ the probability of particle-particle collisions may increase sufficiently quickly that the geometric effect becomes less important than the shielding effect. Thus the shielding effect dominates and the mean force decreases with increasing $\theta$ as shown in Fig. 12(b). Nevertheless, in a denser system such as the one

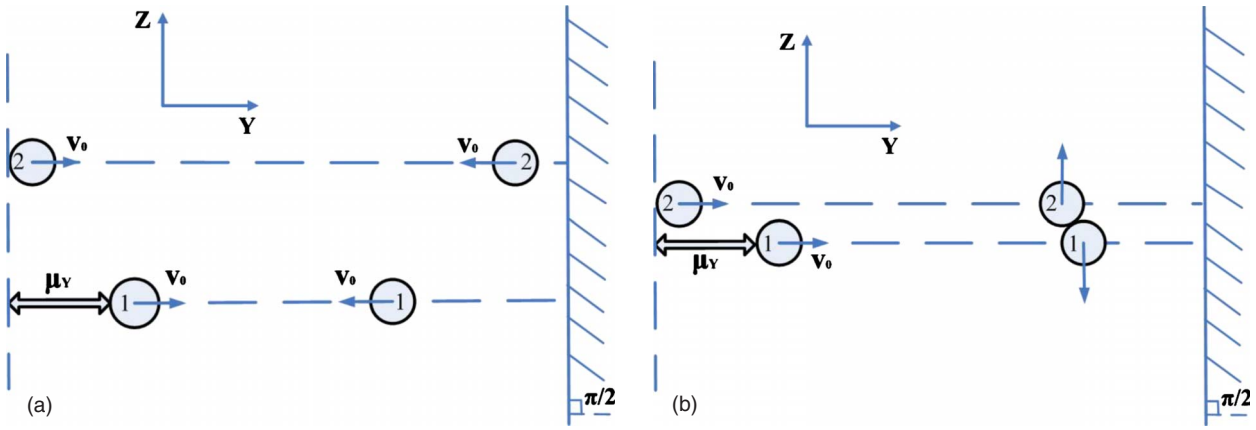


FIG. 13. (Color online) A simplest example of shielding effects. The deflector angle $\theta$ is $\pi/2$. The initial velocity of the two particles is $v_0$, and the particle-wall restitution coefficient $e_w=1$. (a) $B_1$ and $B_2$ are directly rebounded from the wall without any particle-particle collision. The net impulse in this case is $4v_0$. (b) $B_2$ collides with $B_1$, and after the collision, they both scatter to the direction parallel to the wall. The net impulse in this case is $2v_0$. Thus the force experienced by the wall in case (b) is smaller than case (a).

shown in Fig. 12(a), the opposite is true and increasing $\theta$ makes the probability of particle-particle collisions increase so slowly that the geometric effect dominates, and the mean force is monotonically increasing. If one considers a relatively concentrated particle stream, such as the stream in Fig. 12(c), particles have a high probability to collide with each other when $\theta$ is sufficiently large, which implies that the shielding effect reaches its maximum and cannot increase further. Then the geometric effect becomes dominant again and the mean force increases again. Therefore, when $\theta$ increases, even for the simple monotonically increasing case, the fact is that the geometric effect and the shielding effect compete with each other.

In our theoretical analysis, we assume that a given particle in the stream can only experience at most one particle-particle collision. However, in practical situations additional particle-particle collisions can occur. In general, the correlations between particle-particle collisions are weak. In this case, more particles will be scattered by the additional particle-particle collisions and thus leads to stronger shielding. Consequently, our theory will give a useful upper bound for the mean force on the wall (see Figs. 6–11). However, in the very special case $(e\approx 0, \theta\approx \pi/2, S\ll 1)$ in which the particle-particle collisions are strongly correlated, the above argument does not necessarily hold and our theory could underestimate the mean force [see Fig. 11(c)].

In Fig. 14, we show the changes in the theoretical mean force against the particle-particle restitution coefficient $e$. There are also three cases similar to those we have found in our numerical simulations. Figure 14(a) shows that for $V=16$ and $S=0.1$, when the deflector angle $\theta$ is approximately less than 84.5°, increasing the restitution coefficient decreases the mean force experienced by the wall, while Fig. 14(c) shows the opposite case when $\theta$ is approximately larger than 89°. However, Fig. 14(b) shows an interesting case in which $\theta$ is between 84.5° and 89°, the mean force first decreases as $e$ increases, and then increases. Our numerical simulations in Sec. III exactly showed the same qualitative behavior. For a fixed angle $\theta$, the geometric effect $f_g$ does not change. From Eqs. (18), (19), and (22) we can see that when the component of the velocity perpendicular to the wall for the second particle $u_{p2}\geq 0$, $f_s$ is a monotonically decreasing function of the restitution coefficient $e$, while when the component of the velocity perpendicular to the wall for the first particle $u_{p1}\geq 0$, $f_s$ is a monotonically increasing function of the restitution coefficient $e$.

There are two kinds of collisions when two particles collide: "glancing collisions" and "head-on collisions" (see Fig. 15). When a "glancing collision" occurs, the second particle obliquely hits the first particle, and is only slightly deflected by the collision before it hits the wall. In this case, a larger restitution coefficient $e$ increases the deflection of the second particle, thus makes the shielding effect stronger. However, when a "head-on collision" occurs, the first particle is heavily deflected by the second particle and will hit the wall again. In this case, a larger restitution coefficient $e$ means that the first particle will rebound from the particle-particle collision with higher speed and heavy deflection, and thus impart a larger impulse on the wall. This means that increasing $e$ makes the shielding effect weaker. Therefore, if glancing collisions are predominant, the mean force will decrease as $e$ increases, while when head-on collisions are predominant, the mean force will increase as $e$ increases. Hence these two competing effects result in three cases of changes in the mean force against the restitution coefficient.

Varying the value of the particle-wall restitution coefficient $e_w$ does not qualitatively affect the phenomena we have presented, but will weaken both the geometric effect and the shielding effect. Our theory also gives similar results to the cases where $e_w=1$, as shown in Figs. 16 and 17. In fact, the geometric effect in this case can be quantified by the factor $(1+e_w)\sin\theta$ which tells us that the smaller $e_w$ the weaker the geometric effect. This can be seen in Figs. 16 and 17 where a smaller $e_w$ makes the mean force increase more slowly. On the other hand, no matter whether one or both of the particles hits the wall after the possible particle-particle collision, they will be less scattered when $e_w<1$, because a smaller value of $e_w$ makes the first particle slower and the particles have less chance to scatter after the particle-particle collision, thus a smaller value of $e_w$ makes the shielding effect weaker. More-

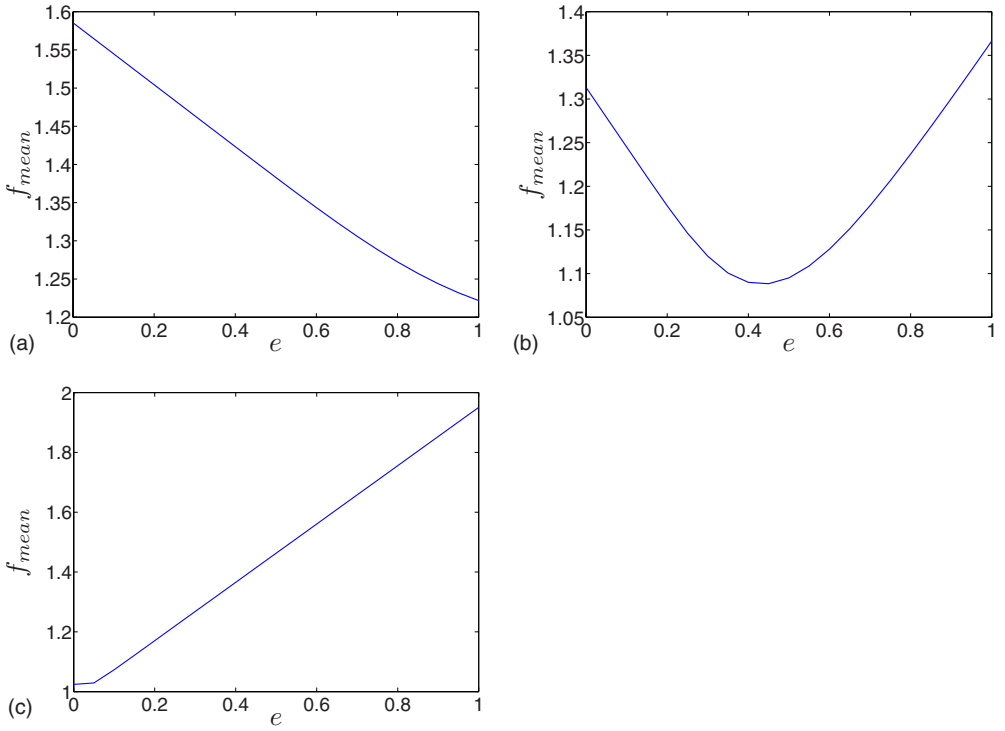


FIG. 14. (Color online) Three cases of the mean force $f_{mean}$ changing against $e$ according to our theoretical results for (a) $\theta=84.5°$; (b) $\theta=86°$, and (c) $\theta=89°$ with $V=16$ and $S=0.1$.

over, the smaller $e_w$ is, the more likely it is that both of the two particles collide with the wall after the collision. This also weakens the shielding effect. This can also be seen in Figs. 16 and 17 where a larger value of $e_w$ can strongly decrease the mean force.

In Sec. IV, the expression for the mean force [Eq. (5)] is based on the assumption that a particle can only experience one particle-particle collision with its nearest neighboring particles. When the collisions with the next nearest neighbor particles are included, the formula (13) gives a correction to

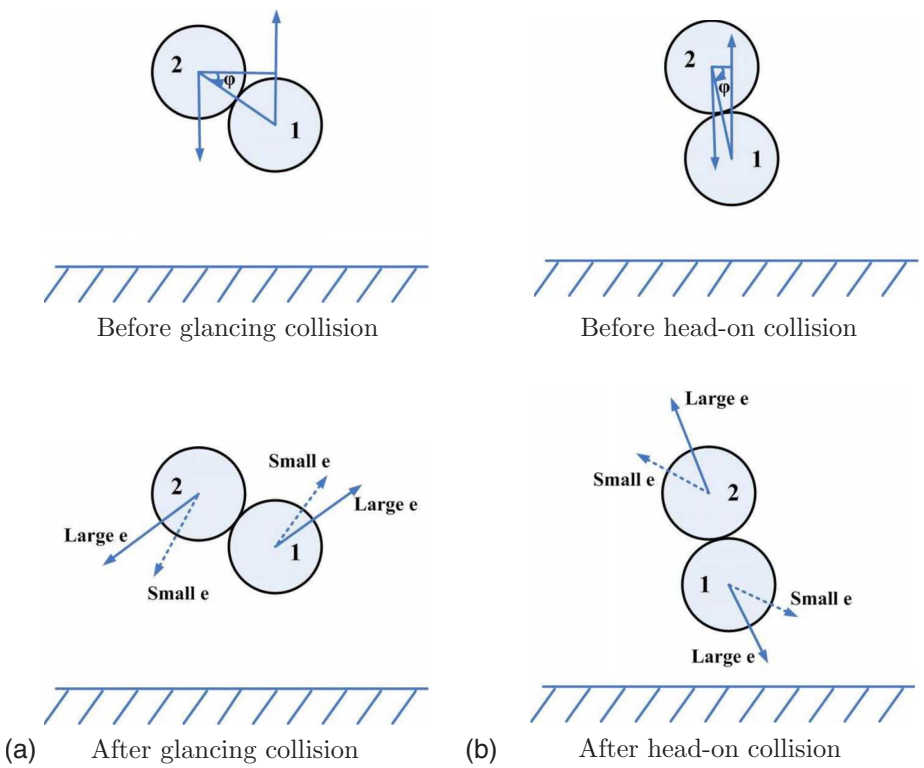


FIG. 15. (Color online) Sketch for (a) "glancing collision" and (b) "head-on collision." When a "glancing collision" occurs, $B_2$ obliquely hits $B_1$, and after the collision $B_2$ is only slightly deflected and hits the wall. In this case, a larger $e$ increases the deflection of $B_2$, thus makes the shielding effect stronger. When a "head-on collision" occurs, $B_1$ is heavily deflected by $B_2$ and will hit the wall again after the collision. In this case, a larger $e$ means that $B_1$ will rebound from the particle-particle collision with higher speed and heavy deflection, and thus makes the shielding effect weaker. Moreover, By the definition of the collision angle $\varphi$ (see Appendix A), we know that when $1-|\cos\varphi| \ll 1$, the particle-particle collision is "glancing collision," while when $|\cos\varphi| \ll 1$ the particle-particle collision is "head-on collision."

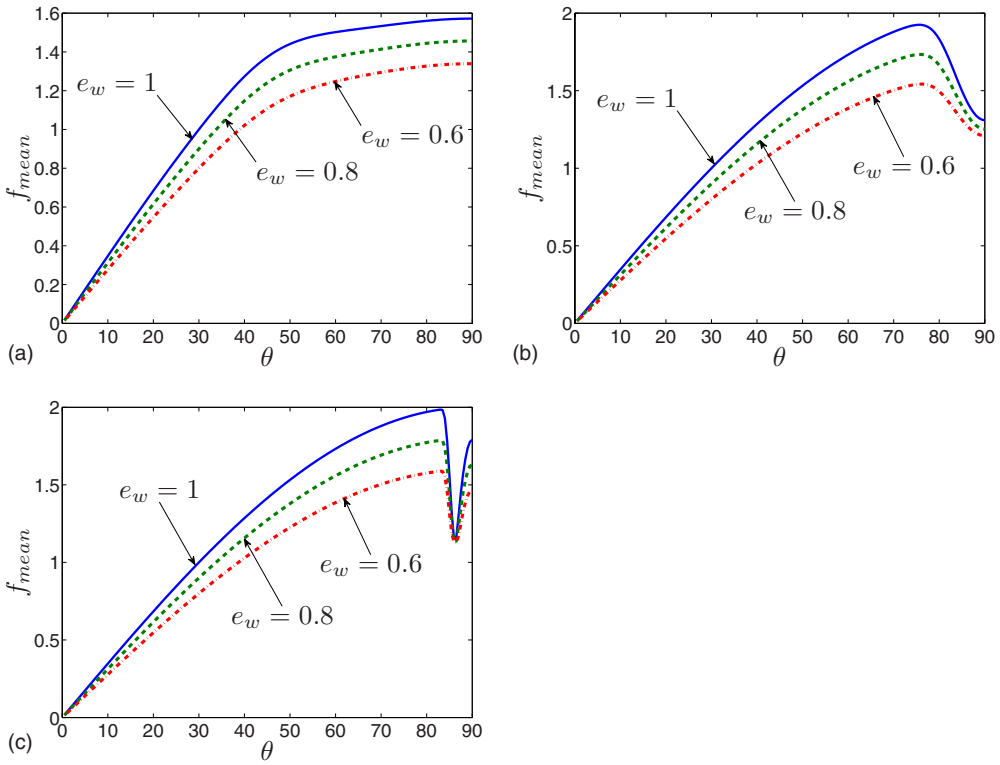


FIG. 16. (Color online) Three cases of the mean force $f_{mean}$ changing against $\theta$ according to our theoretical results for (a) $e_w$=1 (solid blue), $e_w$=0.8 (dashed green) and $e_w$=0.6 (dot dashed red) with $V$=5, $S$=1 and $e$=0.8; (b) $e_w$=1 (solid blue), $e_w$=0.8 (dashed green) and $e_w$=0.6 (dot dashed red) with $V$=20, $S$=1 and $e$=0.2; (c) $e_w$=1 (solid blue), $e_w$=0.8 (dashed green) and $e_w$=0.6 (dot dashed red) with $V$=20, $S$=0.1, and $e$=0.8.

Eq. (5). Figure 18 shows the comparison between the prediction by Eqs. (5) and (13). For a dilute system the correction due to including collisions with the next nearest neighbors is very small. Therefore, in many situations it is sufficient to consider only the collisions with the nearest neighbor.

In our study, we have neglected the effects of gravity. The inclusion of gravity will change the particle trajectories from straight lines to parabolas. If gravity is small, such deviation from the straight line will also be small. In addition, the force experienced by the oblique wall will be sensitive to the initial height of particles because gravity stores some of the kinetic energy in the form of gravitational potential energy, and thus the further particles fall, the larger the impulse the wall experiences. Moreover, in our theory, after particles rebound from the wall, they never hit the wall again unless possible particle-particle collisions occur, thus the force experienced by the wall is not sensitive to the length of the wall. However, this is not the case when gravity is included. With gravity, even if there are no particle-particle collisions in the system, the gravity makes particles hit the wall repeatedly if the wall is sufficiently long. Ultimately, the particle will experience inelastic collapse with the wall and thereafter slide down the wall. In the case of an infinite wall, the wall must support the weight of the particle. The wall must provide a constant force for each particle that has inelastically collapsed and so the mean force increases without bound as the number of particles increases. In order to attain a steady state, it is therefore crucial to have a wall of finite length when gravity is included.

Let $L$ denote the length of the wall and $H$ denote the relative height between initial height of the particles and the midpoint of the wall, as shown in Fig. 19. The system including gravity $g$ can be described by the following dimensionless parameters:

$$\theta,\ e,\ e_w,\ S = \frac{\sigma_Z}{a},\quad \ell = \frac{L}{a},\quad R = \frac{L}{H},\quad G = \frac{g\mu_Y^2}{av_0^2},$$

$$U = \frac{\tau\sqrt{v_0^2 + 2gH}}{a}.$$

The parameters $\theta$, $e$, $e_w$, $S$ have the same meanings as the case without gravity. The parameter $\ell$ is the dimensionless length of the wall. The parameter $R$ is the ratio of the length $L$ and the particles' initial height $H$. The parameter $G$ is the dimensionless gravity and is twice the distance between two neighboring particles when the second particle is first released. The parameter $U$ is the dimensionless velocity of a particle, which is released from the mean location of the stream, immediately before it hits the wall, and $U-G/2$ is the typical distance between itself and the next particle at this time.

Including gravity may cause particles to collide with the wall repeatedly until the particles pass the end of the wall. One can show that, in this case, multiple particle-wall collisions can cause the mean force on the wall to oscillate as $\theta$ varies. A example of the mean force oscillation caused by repeated particle-wall collisions is shown in Fig. 20. By per-

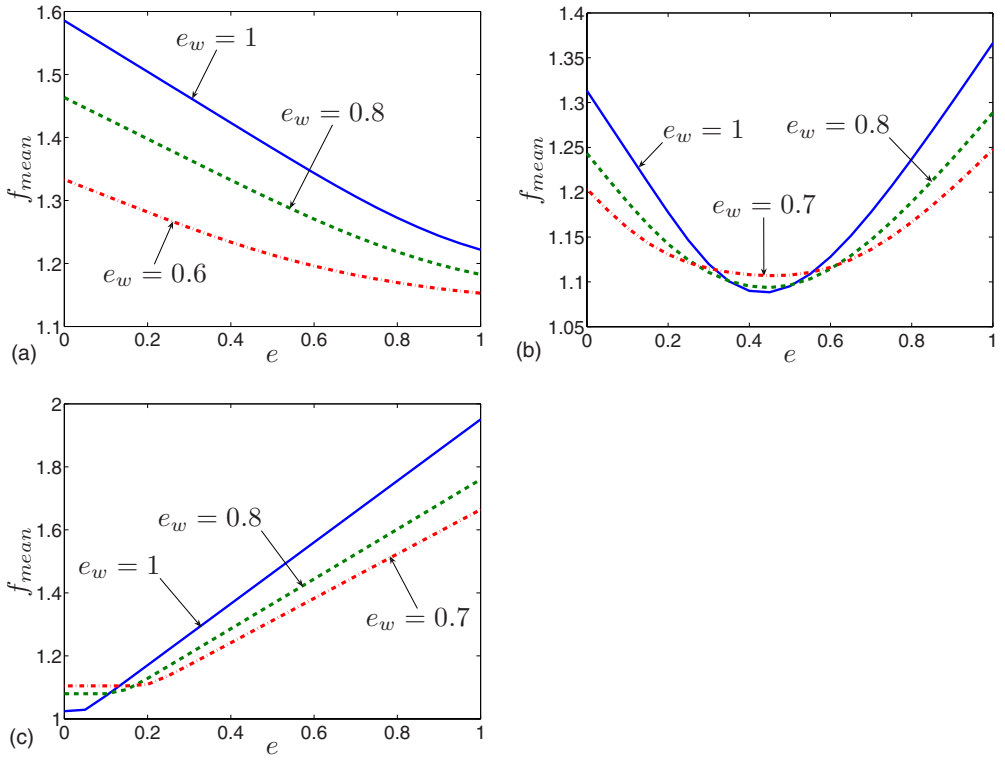


FIG. 17. (Color online) Three cases of the mean force $f_{mean}$ changing against $e$ according to our theoretical results for (a) $e_w$=1 (solid blue), $e_w$=0.8 (dashed green) and $e_w$=0.6 (dot dashed red) with $\theta$=84.5°; (b) $e_w$=1 (solid blue), $e_w$=0.8 (dashed green) and $e_w$=0.7 (dot dashed red) with $\theta$=86°; (c) $e_w$=1 (solid blue), $e_w$=0.8 (dashed green) and $e_w$=0.7 (dot dashed red) with $\theta$=89°. The other parameters are $V$=16 and $S$=0.1.

forming some calculation, one can easily show that in the case where $R \ll \alpha = 16 \cos\theta(e_w^2 \sin^2\theta + \cos^2\theta)$ or in the case where $R \gg \alpha$ and $G \ll \frac{U^2}{2\ell}$, most of the particles will not hit the wall for the second time unless they are deflected by the particle-particle collisions. In this case, the gravity does not play a significant role for the changes of the mean force. However, when $R \gg \alpha$ and $G \gg \frac{U^2}{2\ell}$, the effect of the gravity has a significant effect on the mean force. In this case, the gravity makes most of the particles hit the wall more than once even if there are no particle-particle collisions, and thus the oscillation of the mean force occurs.

In our simulations, we choose the parameters to avoid the repeated particle-wall collisions mentioned above, and we find that including gravity does not qualitatively affect the nonmonotonic phenomena we have presented. As shown in Fig. 21, there still exist three cases of mean force changing against the deflector angle $\theta$. The behavior of the mean force is still a result of the competition between geometric effects and shielding effects. Thus the gravity does not play a critical role in the changes of the mean force except the case in which the repeated particle-wall collisions occur because of the gravity.

## VII. SUMMARY

In this paper, we have considered a system in which a dilute stream of particles originating from infinity collides with an oblique planar wall. We showed that the mean force experienced by the wall can be a nonmonotonic function of the angle between the stream and the wall. Moreover, the mean force may also be an increasing, decreasing or nonmonotonic function of the restitution coefficient in particle-particle collisions. We developed a theory which gives an exact solution for the mean force on the wall if the system is dilute. The theory showed good agreement with the numerical results, and the surprising phenomena can be explained by the competition between shielding effects and geometric effects. The theory generally provides a useful upper bound for the mean force. We hope that our work will motivate further experimental works. These could be done by using an experimental setting similar to the one Rericha *et al.* [14] used to study a different problem, namely shocks in supersonic sand.

## ACKNOWLEDGMENTS

The work described in this paper was fully supported by the Research Grants Council of Hong Kong Special Administrative Region, China (CityU 102908).

## APPENDIX A: DERIVATION FOR THE ANALYTICAL FORMULA FOR THE MEAN FORCE

From Eqs. (15) and (16), we know that in order to evaluate the mean force $F_{mean}$, one must determine the rebound velocity $\vec{v_b}$, the postcollision velocity $\vec{v_p}$ and the region $A$.

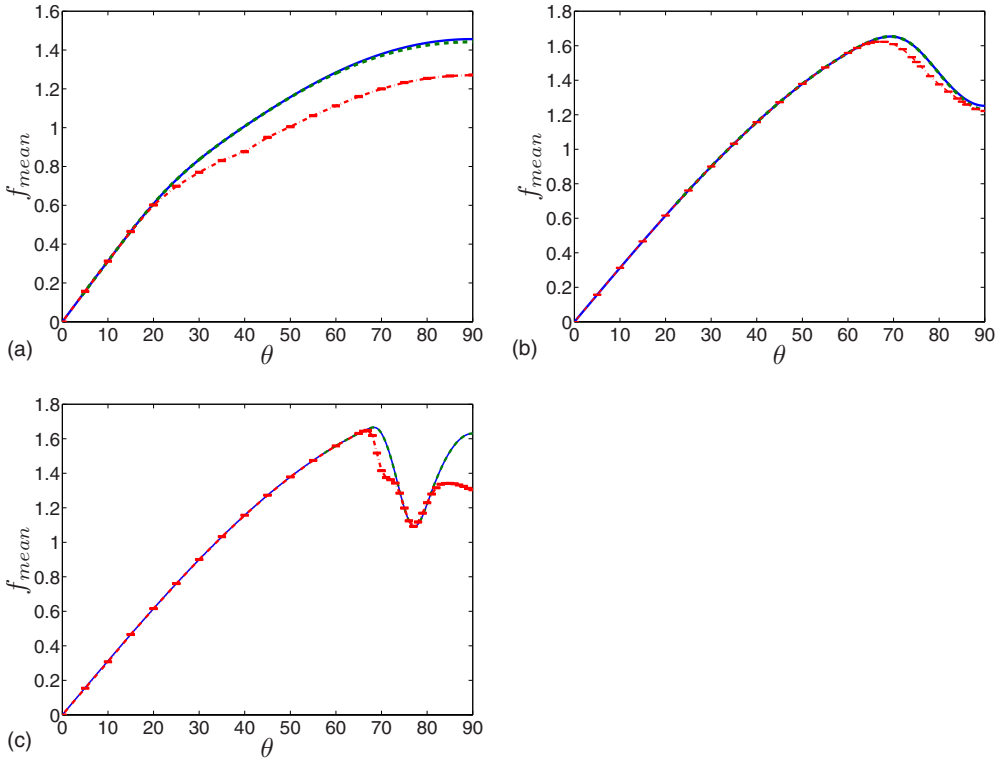


FIG. 18. (Color online) Comparison between the theoretical results for the mean force $f_{mean}$ obtained by $p^{(1)}$ (solid blue) and the results obtained by $p^{(2)}$(dashed green) together with the corresponding numerical results (dot dashed red) for (a) $V=3$, $S=1$, $e=0.8$, and $e_w=0.8$; (b) $V=12$, $S=1$, $e=0.2$ and $e_w=0.8$; (c) $V=6$, $S=0.1$, $e=0.8$, and $e_w=0.8$. In all three cases the solid blue curves and the dashed green curves almost exactly coincide.

For convenience, we can consider a set of geometric transformations as shown in Fig. 22. First we rotate the original system with the deflector angle $\theta$. In this frame [Fig. 22(b)] the two particles have the same velocity components in the direction parallel to the wall. We thus change to a frame moving with this speed as shown in Fig. 22(c).

Figure 23 shows two possible situations when two particles collide. From Fig. 23, we know that the two particles will collide with each other only when the distance between them in the direction parallel to the wall is not more than twice of the particle radius.

Let $\varphi$ denote the angle from the direction $Z'$ [see Fig. 22(c)] to the direction $\overrightarrow{B_2B_1}$ which denotes the vector pointing to $B_1$ from $B_2$, then by geometry we have

$$\cos\varphi = \frac{\mu_Y \cos\theta - (z_2 - z_1)\sin\theta}{2a}, \tag{A1}$$

where $\cos\varphi$ is negative in Fig. 23(a) and positive in Fig. 23(b). Therefore, the two particles will collide with each other if and only if

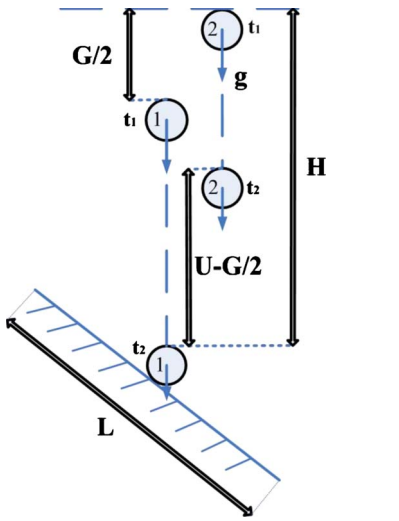


FIG. 19. (Color online) Sketch for the system with gravity.

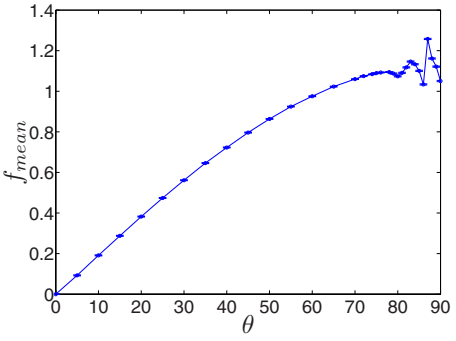


FIG. 20. (Color online) The mean force oscillation caused by repeated particle-wall collisions between about the angle 80° and 90°. The parameters are $G=2$, $R=2$, $\ell=100$, $U=20$, $S=1$, $e=0.6$, and $e_w=1$.

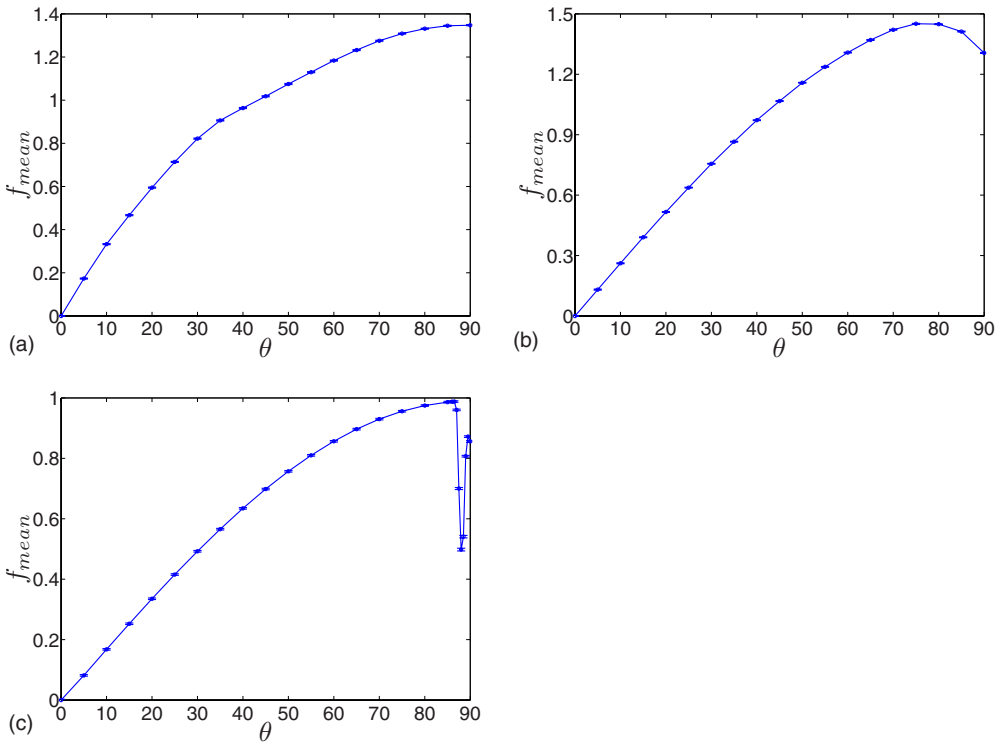


FIG. 21. (Color online) Three cases of the mean force $f_{mean}$ versus the deflector angle $\theta$ when the gravity effect is included for (a) $G=0.02$, $R=0.8$, $\ell=200$, $U=3.16$, $S=3$, $e=0.8$, and $e_w=1$; (b) $G=2$, $R=0.5$, $\ell=450$, $U=60$, $S=5$, $e=0.8$, and $e_w=0.8$; (c) $G=2$, $R=0.5$, $\ell=50$, $U=20$, $S=0.1$, $e=0.8$ and $e_w=1$.

$$|\cos\varphi| \le 1. \tag{A2}$$

Combining Eqs. (A1) and (A2), we obtain

$$A = \left\{ (z_1,z_2) \in \mathbb{R}^2 \left| \frac{\mu_Y \cos\theta - 2a}{\sin\theta} \le z_2 - z_1 \le \frac{\mu_Y \cos\theta + 2a}{\sin\theta} \right. \right\}. \tag{A3}$$

When the two particles do not collide with each other, they will directly rebound from the wall, and thus have the same rebound velocities, i.e., $\overrightarrow{v_{b1}}=\overrightarrow{v_{b2}}$. We define the following operators:

$$R_1 = \begin{pmatrix} \sin\theta & -\cos\theta \\ \cos\theta & \sin\theta \end{pmatrix} \quad C_w = \begin{pmatrix} -e_w & 0 \\ 0 & 1 \end{pmatrix},$$

where $R_1$ denotes the coordinate rotation matrix from $(Y,Z)$ to $(Y',Z')$, as shown in Fig. 22, and $C_w$ denotes the particle-wall collision matrix. By simple geometry it is easy to write the rebound velocities as follows:

$$\overrightarrow{v_{b1}} = \begin{pmatrix} u_{b1} \\ v_{b1} \end{pmatrix} = \overrightarrow{v_{b2}} = \begin{pmatrix} u_{b2} \\ v_{b2} \end{pmatrix} = C_w R_1 \begin{pmatrix} v_0 \\ 0 \end{pmatrix} = \begin{pmatrix} -e_w v_0 \sin\theta \\ v_0 \cos\theta \end{pmatrix}, \tag{A4}$$

where $u_{b1}$, $u_{b2}$, respectively, denote the rebound velocity components perpendicular to the wall for the two particles, and $v_{b1}$, $v_{b2}$, respectively, denote the parallel ones.

When the two particles collide with each other, $B_2$ collides with $B_1$ after $B_1$ rebounds from the wall. Let

$$R_2 = \begin{pmatrix} \cos\varphi & -\sin\varphi \\ \sin\varphi & \cos\varphi \end{pmatrix}$$

denote the rotation matrix by which we can obtain the two particles' velocity components in the directions normal and parallel to the line of their centers before the particle-particle collision. This allows us to apply inelastic collision rules and solve for the postcollision velocities in a simple way. Let $v_{1n}$, $v_{2n}$, respectively, denote the norm components mentioned above, and $v_{1c}$, $v_{2c}$, respectively, denote the parallel ones, then we obtain

$$\begin{pmatrix} v_{1n} \\ v_{1c} \end{pmatrix} = R_2 C_w R_1 \begin{pmatrix} v_0 \\ 0 \end{pmatrix} = \begin{pmatrix} (-e_w \sin\theta\cos\varphi - \cos\theta\sin\varphi)v_0 \\ (-e_w \sin\theta\sin\varphi + \cos\theta\cos\varphi)v_0 \end{pmatrix},$$

$$\begin{pmatrix} v_{2n} \\ v_{2c} \end{pmatrix} = R_2 R_1 \begin{pmatrix} v_0 \\ 0 \end{pmatrix} = \begin{pmatrix} (\sin\theta\cos\varphi - \cos\theta\sin\varphi)v_0 \\ (\sin\theta\sin\varphi + \cos\theta\cos\varphi)v_0 \end{pmatrix}.$$

Since there is no friction, the components of velocity perpendicular to the line of centers of the two particles are unchanged by the collision. By the definition of the restitution coefficient $e$, and the conservation of momentum, the rules also allow us to determine the post-collision velocities $\overrightarrow{v_{p1}}$ and $\overrightarrow{v_{p2}}$ by using the particle-particle collision matrix

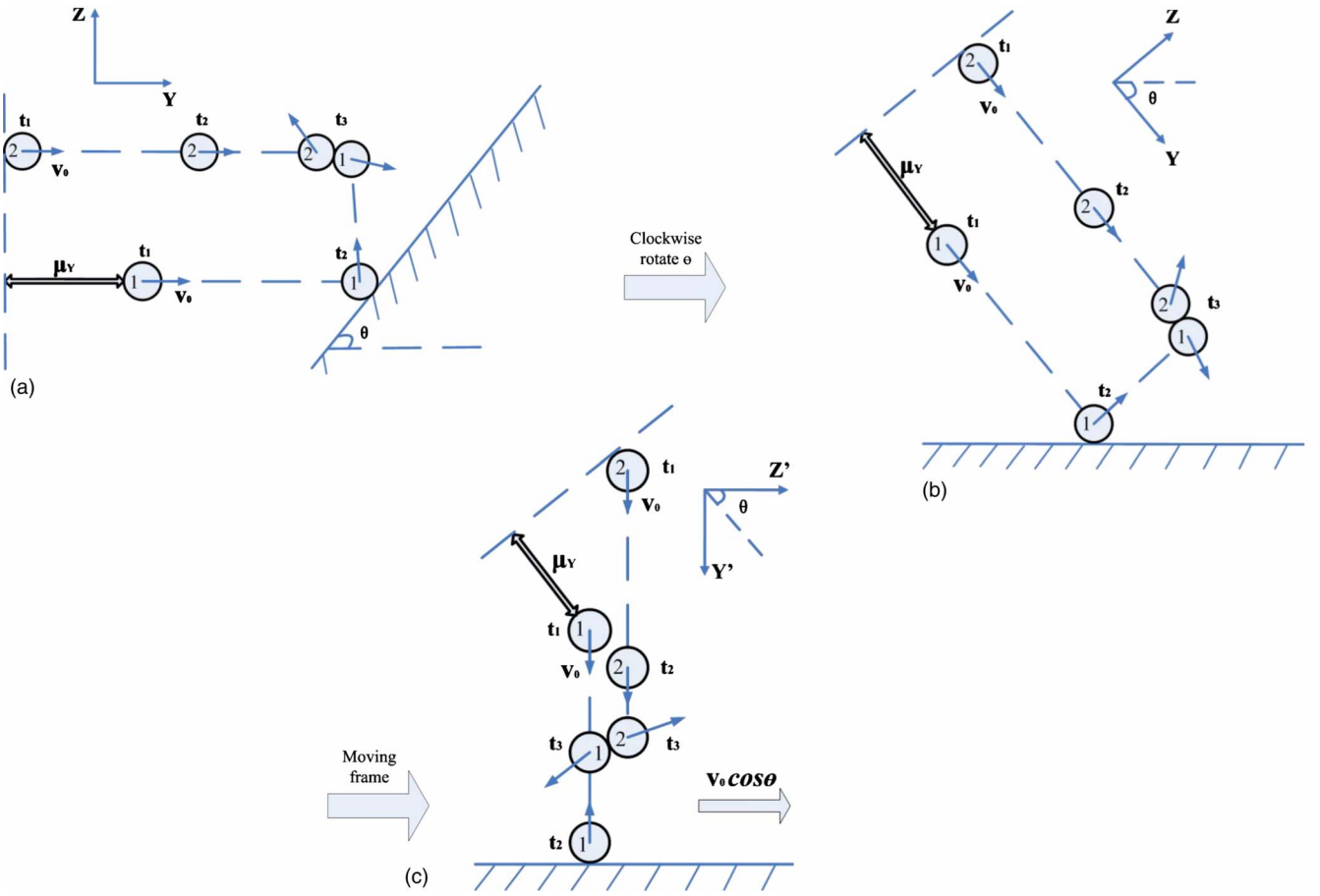


FIG. 22. (Color online) Rotation for the system. We can clockwise rotate the original system (a) with the deflector angle $\theta$ to obtain the system (b), and then for convenience we can investigate pairwise particle collision in a moving frame as shown in (c).

$$C_p = \begin{pmatrix} \frac{1-e}{2} & \frac{1+e}{2} \\ \frac{1+e}{2} & \frac{1-e}{2} \end{pmatrix}.$$

Let $v'_{1n}$, $v'_{2n}$, $v'_{1c}$, and $v'_{2c}$, respectively, denote the counterparts of $v_{1n}$, $v_{2n}$, $v_{1c}$ and $v_{2c}$ after the particle-particle collision, then we have

$$\begin{pmatrix} v'_{1n} \\ v'_{2n} \end{pmatrix} = \begin{pmatrix} v_{1n} \\ v_{2n} \end{pmatrix},$$

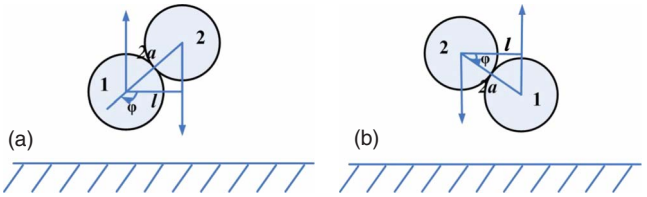


FIG. 23. (Color online) Two possible cases when two particles collide with each other. (a) shows the case in which the particle-particle collision angle $\varphi$ is an obtuse angle. (b) shows the case in which the particle-particle collision angle $\varphi$ is an acute angle.

$$\begin{pmatrix} v'_{1c} \\ v'_{2c} \end{pmatrix} = C_p \begin{pmatrix} v_{1c} \\ v_{2c} \end{pmatrix}.$$

Therefore, multiplying the inverse of the rotation matrix $R_2$ gives the post-collision velocities $\overrightarrow{v_{p1}}$ and $\overrightarrow{v_{p2}}$ in the coordinate $(Y', Z')$ as follows:

$$\overrightarrow{v_{p1}} = \begin{pmatrix} u_{p1} \\ v_{p1} \end{pmatrix} = R_2^{-1} \begin{pmatrix} v'_{1n} \\ v'_{1c} \end{pmatrix},$$

$$\overrightarrow{v_{p2}} = \begin{pmatrix} u_{p2} \\ v_{p2} \end{pmatrix} = R_2^{-1} \begin{pmatrix} v'_{2n} \\ v'_{2c} \end{pmatrix},$$

where $u_{p1}$ and $u_{p2}$, respectively, denote the post-collision velocity components perpendicular to the wall for the two particles, and $v_{p1}$ and $v_{p2}$, respectively, denote the parallel components. Thus we obtain

$$u_{p1} = v_0 \sin\theta \left[ -e_w q^2 + \left( \frac{1+e}{2} - \frac{1-e}{2} e_w \right) p^2 \right], \quad \text{(A5)}$$

$$u_{p2} = v_0 \sin\theta \left[ q^2 + \left( \frac{1-e}{2} - \frac{1+e}{2} e_w \right) p^2 \right], \quad \text{(A6)}$$

$$v_{p1} = v_0\left[\frac{1+e}{2}(1+e_w)pq\ \sin\ \theta + \cos\ \theta\right], \tag{A7}$$

$$v_{p2} = v_0\left[-\frac{1+e}{2}(1+e_w)pq\ \sin\ \theta + \cos\ \theta\right], \tag{A8}$$

where

$$q = \cos\ \varphi = \frac{\mu_Y\ \cos\ \theta - (z_2 - z_1)\sin\ \theta}{2a}$$

and

$$p = \sin\ \varphi = \sqrt{1-q^2}.$$

In fact, it is easy to see that only the velocity components perpendicular to the wall will give impulse to the oblique wall, while the parallel components will not contribute to the impact on the wall, thus by using the particle-wall collision matrix $C_w$, we can determine the post-particle-wall collision velocity for the particles which obtain positive velocity components perpendicular to the wall after their particle-particle collision. Actually, Eqs. (A5) and (A6) tell us that when $0 \le e_w \le \frac{1-e}{1+e}$, $B_2$ will definitely hit the wall again, while when $\frac{1-e}{1+e} < e_w \le 1$, either one or both of $B_1$ and $B_2$ may hit. Let $\xi = \frac{z_2 - z_1}{\sqrt{2}\sigma_Z}$, then we have

$$q = \cos\ \varphi = \frac{\mu_Y \cos\ \theta - \sqrt{2}\xi\sigma_Z\ \sin\ \theta}{2a}$$

$$= \frac{V\ \cos\ \theta - \sqrt{2}\xi S\ \sin\ \theta}{2}, \quad \xi \in \mathbb{R}.$$

Through the above linear transform, and combining Eqs. (5), (15), and (16), we can write the dimensionless mean force $f_{mean}$ as follows:

$$f_{mean} = \frac{F_{mean}}{mv_0^2/\mu_Y} = \frac{1}{1+p_\tau}(f_w + f_{cw}), \tag{A9}$$

$$p_\tau = \int_\Omega \rho(\xi)d\xi, \tag{A10}$$

$$f_w = \frac{\widetilde{F}_w}{mv_0^2/\mu_Y} = (1+e_w)\sin\ \theta, \tag{A11}$$

$$f_{cw} = \frac{\widetilde{F}_{cw}}{mv_0^2/\mu_Y} = (1+e_w)\left(\int_\Omega \mathbf{1}_{\Lambda_1}\left|\frac{u_{p1}}{v_0}\right|\rho(\xi)d\xi + \int_\Omega \mathbf{1}_{\Lambda_2}\left|\frac{u_{p2}}{v_0}\right|\rho(\xi)d\xi\right), \tag{A12}$$

where $f_w$ and $f_{cw}$, respectively, denote the dimensionless average impact on the wall caused by the rebound velocity and the postcollision velocity. The quantities $\mathbf{1}_{\Lambda_i}(i=1,2)$ denote the indicator functions of the sets

$$\Lambda_i = \{\xi \in \mathbb{R} | u_{pi} \ge 0\} \quad (i=1,2). \tag{A13}$$

The interval,

$$\Omega = \left[\frac{V\cos\ \theta - 2}{\sqrt{2}S\ \sin\ \theta}, \frac{V\cos\ \theta + 2}{\sqrt{2}S\ \sin\ \theta}\right] \tag{A14}$$

is the phase set of $A$ formulated in Eq. (A3) under the linear transform $\xi = \frac{z_2 - z_1}{\sqrt{2}\sigma_Z}$, and we can write the joint distribution density $\rho(z_1, z_2)$ as a function of the variable $\xi$, i.e., $\rho(\xi)$. If we choose the marginal density function of the $Z$-location of particles $\rho_Z$ to be a Gaussian distribution with mean zero and standard deviation $\sigma_Z$, we can obtain the exact distribution density for the standardized relative distance of the two particles' initial height

$$\rho(\xi) = \frac{1}{\sqrt{2\pi}}\exp\left(-\frac{\xi^2}{2}\right). \tag{A15}$$

Therefore, substituting Eqs. (A5), (A6), (A14), and (A15) into Eq. (A12), and combining Eqs. (A9) and (A11), we obtain the analytical formula of dimensionless mean force $f_{mean}$ Eq. (17).

## APPENDIX B

### 1. Derivation that the probability of a particle experiencing a particle-particle collision is low if $V\cos\theta \gg 1$

Let $P$ denote the probability of a particle, say $B_n$, experiencing a particle-particle collision, and let $p_i$ denote the probability of $B_n$ experiencing a particle-particle collision with the particle $B_{n-i}$ $(i \in \mathbb{Z})$. Then we can write $P$ as

$$P = \sum_{i=-\infty}^{+\infty} \mathbb{P}(C_{n,n-i}) = 2\sum_{i=1}^{+\infty} \mathbb{P}(C_{n,n-i}) = 2\sum_{i=1}^{+\infty} p_i.$$

Our theory assumes that each particle can experience only one particle-particle collision. Let $A_i$ denote the set of events that guarantee $B_n$ may collide with $B_{n-i}$ under our assumption. In the theoretical derivation in Sec. IV, we have obtained that

$$A_1 = \overline{D_{n-1}},$$

$$A_2 = \overline{D_{n-2}} \cap \overline{C_{n-1,n-2}} \cap \overline{C_{n,n-1}}.$$

And we can obtain the expressions for $A_i$ through a similar approach. We can also write $p_i$ as

$$p_i = \mathbb{P}(C_{n,n-i}) = \mathbb{P}(C_{n,n-i} \cap A_i).$$

Then we have

$$P = 2\sum_{i=1}^{+\infty} p_i = 2\sum_{i=1}^{+\infty} \mathbb{P}(C_{n,n-i} \cap A_i) \le 2\sum_{i=1}^{+\infty} \mathbb{P}(C_{n,n-i}|A_i) = 2\sum_{i=1}^{+\infty} p_{i\tau}$$

where $p_{i\tau} = \mathbb{P}(C_{n,n-i}|A_i)$. Similar to the derivation in Sec. IV, we can obtain

$$p_{i\tau} = \mathbb{P}(C_{n,n-i}|A_i) = \int_{\Omega_i} \rho(\xi)d\xi,$$

where

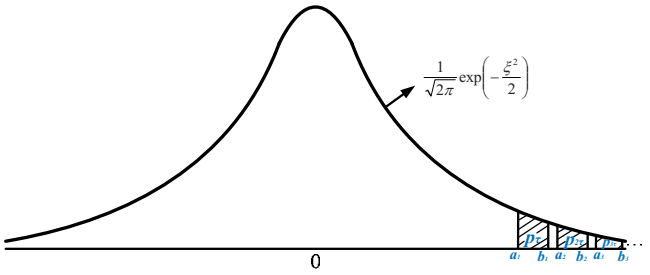


FIG. 24. (Color online) Sketch for the terms of the series $\Sigma_{i=1}^{+\infty}p_{i\tau}$ in the case where $V\cos\theta \gg 1$ and $\frac{V\cos\theta}{S\sin\theta} \gg 1$. All the terms $p_{i\tau}$ are integrals on the intervals which locate on the tail of the standard normal distribution.

$$\rho(\xi) = \frac{1}{\sqrt{2\pi}}\exp\left(-\frac{\xi^2}{2}\right)$$

and

$$\Omega_i = \left[\frac{iV\cos\theta - 2}{\sqrt{2}S\sin\theta}, \frac{iV\cos\theta + 2}{\sqrt{2}S\sin\theta}\right].$$

We can see that $p_{i\tau}$ is a integral of the density of standard normal distribution on an interval with center $\frac{iV\cos\theta}{\sqrt{2}S\sin\theta}$ and length $\frac{4}{\sqrt{2}S\sin\theta}$. We will divide $V\cos\theta \gg 1$ into two cases to show that the series $\Sigma_{i=1}^{+\infty}p_{i\tau}$ is convergent and the sum is much small than 1, thus the probability of a particle experiencing a particle-particle collision $P$ is low.

**Case 1:** $V\cos\theta \gg 1$ and $\frac{V\cos\theta}{S\sin\theta} \gg 1$

In this case, all the terms in the series $\Sigma_{i=1}^{+\infty}p_{i\tau}$ are integrals on the intervals which locate on the tail of the standard normal distribution (see Fig. 24). We use the following inequality as the estimation for the tail probability of the standard normal distribution,

$$\mathbb{P}(\mathbb{X} \geq x) \leq \frac{1}{\sqrt{2\pi x}}\exp\left(-\frac{x^2}{2}\right),$$

where $\mathbb{X}$ is a random variable with standard normal distribution. Let

$$a_i = \frac{iV\cos\theta - 2}{\sqrt{2}S\sin\theta} \quad \text{and} \quad b_i = \frac{iV\cos\theta + 2}{\sqrt{2}S\sin\theta}. \tag{B1}$$

They are both monotonically increasing functions of the index $i$. And if $V\cos\theta \gg 1$, then $b_i < a_{i+1}$ since $a_{i+1} - b_i = \frac{V\cos\theta - 4}{\sqrt{2}S\sin\theta} > 0$ in this case. Hence none of the shaded areas in Fig. 24 overlaps. And notice that

$$\frac{1}{a_1} = \frac{\sqrt{2}S\sin\theta}{V\cos\theta - 2} \ll 1 \quad \text{and} \quad \exp\left(-\frac{a_1^2}{2}\right) \ll 1,$$

then we can obtain

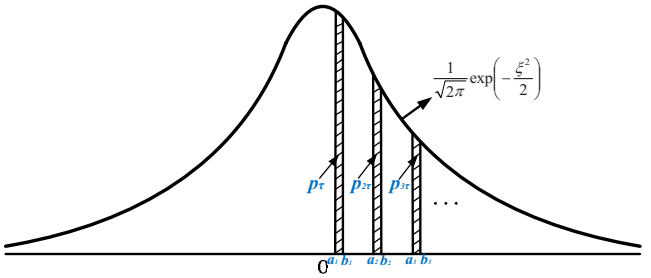


FIG. 25. (Color online) Sketch for the terms of the series $\Sigma_{i=1}^{+\infty}p_{i\tau}$ in the case where $V\cos\theta \gg 1$ and $S\sin\theta \gg 1$. All the terms $p_{i\tau}$ are integrals of the standard normal distribution on the intervals with thin length.

$$\begin{aligned}\sum_{i=1}^{+\infty} p_{i\tau} &= \sum_{i=1}^{+\infty}\int_{\Omega_i}\rho(\xi)d\xi \\ &= \sum_{i=1}^{+\infty}\mathbb{P}(a_i \leq \mathbb{X} \leq b_i) \leq \mathbb{P}(\mathbb{X} \geq a_1) \\ &\leq \frac{1}{\sqrt{2\pi}a_1}\exp\left(-\frac{a_1^2}{2}\right) \ll 1.\end{aligned}$$

Hence the series $s = \Sigma_{i=1}^{+\infty}p_{i\tau}$ is convergent and the sum $s \ll 1$. Therefore, we can obtain

$$P \leq 2\sum_{i=1}^{+\infty} p_{i\tau} = 2s \ll 1.$$

**Case 2:** $V\cos\theta \gg 1$ and $S\sin\theta = O(V\cos\theta)$

In this case, we have $S\sin\theta \gg 1$ which implies all the terms in the series $\Sigma_{i=1}^{+\infty}p_{i\tau}$ are integrals of the standard normal distribution on the intervals with thin length (see Fig. 25). We use the following inequality as the estimation for the probability over these regions,

$$\mathbb{P}(a_i \leq \mathbb{X} \leq b_i) \leq \frac{b_i - a_i}{\sqrt{2\pi}}\exp\left(-\frac{a_i^2}{2}\right) \quad (0 \leq a_i \leq b_i).$$

Then we can obtain

$$\begin{aligned}\sum_{i=1}^{+\infty} p_{i\tau} &= \sum_{i=1}^{+\infty}\int_{\Omega_i}\rho(\xi)d\xi \\ &= \sum_{i=1}^{+\infty}\mathbb{P}(a_i \leq \mathbb{X} \leq b_i) \leq \sum_{i=1}^{+\infty}\frac{2}{\sqrt{\pi}S\sin\theta}\exp\left(-\frac{a_i^2}{2}\right) \\ &\leq \frac{2}{\sqrt{\pi}S\sin\theta}\cdot\sum_{i=1}^{+\infty}\exp\left(-\frac{a_i^2}{2}\right) \\ &\leq \frac{2}{\sqrt{\pi}S\sin\theta}\cdot\int_0^{+\infty}\exp\left[-\left(\frac{xV\cos\theta - 2}{\sqrt{2}S\sin\theta}\right)^2\right]dx \\ &= \frac{2}{\sqrt{\pi}S\sin\theta}\cdot\frac{\sqrt{2\pi}S\sin\theta}{2V\cos\theta}\cdot\left[\operatorname{erf}\left(\frac{\sqrt{2}}{S\sin\theta}\right)\right. \\ &\quad \left. + \lim_{x\to+\infty}\operatorname{erf}\left(\frac{xV\cos\theta - 2}{\sqrt{2}S\sin\theta}\right)\right] \leq \frac{2\sqrt{2}}{V\cos\theta}.\end{aligned}$$

In this case, $V\cos\theta \gg 1$, thus the series $s=\sum_{i=1}^{+\infty} p_{i\tau}$ is convergent and the sum $s \ll 1$. Therefore, we can obtain

$$P \le 2\sum_{i=1}^{+\infty} p_{i\tau} = 2s \ll 1.$$

Now combining the two cases, we can conclude that the probability of a particle experiencing a particle-particle collision $P$ is low if $V\cos\theta \gg 1$.

#### 2. Derivation that the probability of a given particle experiencing two particle-particle collisions is low if $V \gg 1$ and $V \gg S$

In this subsection, we will show that if $V \gg 1$ and $V \gg S$, the probability of any given particle, say the $n$th particle $B_n$, experiencing two particle-particle collisions is low.

We therefore define

$Q = \mathbb{P}(B_n$ experiences two particle-particle collisions).

Assume that $B_n$ has already experienced its first particle-particle collision with some particle in the stream. Then, we bound the probability $Q$ as follows:

$$\begin{aligned} Q &= \mathbb{P}(B_n \text{ experiences a second collision} | B_n \\ &\quad \text{experiences a first collision}) \\ &\quad \times \mathbb{P}(B_n \text{ experiences a first collision}) \\ &\le \mathbb{P}(B_n \text{ experiences a second collision} | B_n \\ &\quad \text{experiences the first collision}). \end{aligned}$$

We define

$$\begin{aligned} \tilde{Q} &= \mathbb{P}(B_n \text{ experiences a second collision} | B_n \\ &\quad \text{experiences the first collision}), \end{aligned}$$

which represents the probability of $B_n$ experiencing another particle-particle collision given that it has already experienced its first particle-particle collision.

In order to obtain the exact expression for the probability $\tilde{Q}$, for each particle that may collide with $B_n$, we need to perform multiple integrals with respect to the positions and velocities of the two particles over a domain which represents the condition for the collision.

The derivation for the exact formula for $\tilde{Q}$ is complicated. Therefore we will estimate the order of magnitude of the probability $\tilde{Q}$. Starting from the position immediately after its first collision, the particle $B_n$ will pass through the particle stream with its post-collision velocity and may experience a second particle-particle collision. For our estimation of the order of magnitude of $\tilde{Q}$, we assume that $B_n$ passes through the stream from $-\infty$ to $+\infty$ in the $Z$ direction. The angle between the velocities of $B_n$ and the stream will have a certain distribution. In order to obtain an order of magnitude estimate, we choose a uniformly distributed angle which we denote by $\eta (0 \le \eta \le \pi)$. That is, the density function of $\eta$ is given by

$$\rho_\eta(\eta) = \begin{cases} \dfrac{1}{\pi} & \text{if } \eta \in [0,\pi] \\ 0 & \text{otherwise} \end{cases}. \tag{B2}$$

The post-collision speed of the particle $B_n$ will be of order unity. In order to obtain an order of magnitude estimate we assume that $B_n$ passes through the stream with velocity $(\cos\eta, \sin\eta)^{\mathrm{T}}$. In addition, the particles in the stream move forward with velocity $(1,0)^{\mathrm{T}}$. We let $\Gamma$ denote the probability of $B_n$ experiencing another particle-particle collision in this case. Then the probability $\Gamma$ provides an estimate for the order of magnitude of the probability $\tilde{Q}$.

By symmetry, we only consider the case in which the $Z$-location of $B_n$ is non-negative. That is, $B_n$ is initially located at $Z=0$ and then passes through the particle stream from 0 to $+\infty$ in the $Z$ direction. In this case, let $\delta y$ denote the relative distance between the initial $Y$ location of $B_n$ and $B_{k+1}$ which represents the nearest neighboring particle to $B_n$. In order to obtain an order of magnitude estimate, we choose a uniform distribution for the relative distance $\delta y$. That is, the density function of $\delta y$ is given by

$$\rho_y(\delta y) = \begin{cases} \dfrac{1}{\mu_Y} & \text{if } \delta y \in [0,\mu_Y] \\ 0 & \text{otherwise} \end{cases}. \tag{B3}$$

As before, the density function of the $Z$ location of the particles in the stream is given by

$$\rho_z(z) = \frac{1}{\sqrt{2\pi}\sigma_Z}\exp\left(-\frac{z^2}{2\sigma_Z^2}\right). \tag{B4}$$

Next we bound the probability $\Gamma$ to obtain the order of magnitude estimation for the probability $\tilde{Q}$. We therefore define $\Gamma_j = \mathbb{P}(C_{n,k+j})(j \in \mathbb{Z})$ which represents the probability of $B_n$ experiencing a particle-particle collision with $B_{k+j}$. Then we can write the probability $\Gamma$ as

$$\Gamma = 2\sum_{j=1}^{+\infty}\prod_{i=0}^{j-1}(1-\Gamma_i)\Gamma_j \tag{B5}$$

where

$$\Gamma_0 = 0, \quad \Gamma_j = \int\int\int_{\Omega_j} \psi(\delta y, z, \eta)\, d\delta y\, dz\, d\eta \quad (j \ge 1, j \in \mathbb{Z}), \tag{B6}$$

$$\Omega_j = \left\{ (\delta y, z, \eta) \,\middle|\, \left| \delta y \cos\tfrac{\eta}{2} - z\sin\tfrac{\eta}{2} + (j-1)\mu_Y \cos\tfrac{\eta}{2} \right| \le 2a \right\}. \tag{B7}$$

The quantity $\psi(\delta y, z, \eta) = \rho_y(\delta y)\cdot\rho_z(z)\cdot\rho_\eta(\eta)$ represents the joint density function of $\delta y$, $z$, and $\eta$, which for the purposes of obtaining an order of magnitude estimate we assume are independent. The set $\Omega_j (j \ge 1, j \in \mathbb{Z})$ represents the conditions for $B_n$ experiencing a particle-particle collision with $B_{k+j}$.

Note that when the particle $B_n$ moves in the direction almost opposite to the direction of the particle stream (the

angle $\eta$ is close to $\pi$), then the probability of a collision will be large. We therefore divide the integrals in Eq. (B5) into two cases: angles close to $\pi$ and those bounded away from $\pi$. We let $\varepsilon$ denote a small positive number and performing some integrals, we can bound the probability $\Gamma$ as follows:

$$\Gamma \leq \frac{2}{\pi}\sum_{j=1}^{+\infty}\int\int\int_{\Omega_j}\psi \mathbf{1}_{[0,\pi-\varepsilon]}(\eta)d\delta dy dz d\eta + O(\varepsilon) \quad \text{(B8)}$$

$$= \frac{2}{\pi}\sum_{j=1}^{+\infty}\int_0^{\pi-\varepsilon}\gamma_j(\eta)d\eta + O(\varepsilon) \quad \text{(B9)}$$

where $\mathbf{1}_{[0,\pi-\varepsilon]}(\eta)$ denotes the indicator function of the interval $[0,\pi-\varepsilon]$, i.e.,

$$\mathbf{1}_{[0,\pi-\varepsilon]}(\eta) = \begin{cases} 1 & \text{if } \eta \in [0,\pi-\varepsilon] \\ 0 & \text{otherwise} \end{cases}$$

and

$$\gamma_j(\eta) = \alpha_j^+(\eta) - \alpha_j^-(\eta) + \beta_j^+(\eta) - \beta_j^-(\eta) + \beta_{j-1}^-(\eta) - \beta_{j-1}^+(\eta) + \lambda_j(\eta),$$

$$\alpha_j^{\pm}(\eta) = \frac{(j-1)V\cos\frac{\eta}{2} \pm 2}{V\cos\frac{\eta}{2}}\left[\operatorname{erf}\left(\frac{jV\cos\frac{\eta}{2}\pm 2}{\sqrt{2}S\sin\frac{\eta}{2}}\right) - \operatorname{erf}\left(\frac{(j-1)V\cos\frac{\eta}{2}\pm 2}{\sqrt{2}S\sin\frac{\eta}{2}}\right)\right],$$

$$\beta_j^{\pm}(\eta) = \frac{\sqrt{2}S\sin\frac{\eta}{2}}{\sqrt{\pi}V\cos\frac{\eta}{2}}\exp\left[-\left(\frac{jV\cos\frac{\eta}{2}\pm 2}{\sqrt{2}S\sin\frac{\eta}{2}}\right)^2\right],$$

$$\lambda_j(\eta) = \operatorname{erf}\left(\frac{jV\cos\frac{\eta}{2}+2}{\sqrt{2}S\sin\frac{\eta}{2}}\right) - \operatorname{erf}\left(\frac{jV\cos\frac{\eta}{2}-2}{\sqrt{2}S\sin\frac{\eta}{2}}\right).$$

If $V \gg 1$ and $V \gg S$, by letting $\varepsilon = \frac{1}{V}$ and performing some elementary calculations, one can show that the series $\Sigma_{j=1}^{+\infty}\gamma_j(\eta)$ is uniformly convergent with respect to the angle $\eta$, and the magnitude of the expression given by Eq. (B9) is $O(\frac{S}{V})$. Then, $\Gamma \ll 1$, and thus the probability of a given particle experiencing two particle-particle collisions is low.


[1] R. Behringer, Chaos **9**, 509 (1999).
[2] W. Peng and D. F. Parker, J. Fluid Mech. **333**, 231 (1997).
[3] L. H. Wiryanto and E. O. Tuck, J. Aust. Math. Soc. Ser. B, Appl. Math. **41**, 458 (2000).
[4] P. Christodoulides and F. Dias, J. Fluid Mech. **621**, 243 (2009).
[5] J. D. Anderson, Jr., *Modern Compressible Flow with Historical Perspective* (McGraw-Hill Publishing Company, Boston, 1990).
[6] V. Kamenetsky, A. Goldshtein, M. Shapiro, and D. Degani, Phys. Fluids **12**, 3036 (2000).
[7] A. M. Worthington, *A Study of Splashes* (Longmans, Green and Co., London, 1908).
[8] S. T. Thoroddsen and Q. Amy, Phys. Fluids **13**, 4 (2001).
[9] H. M. Jaeger, S. R. Nagel, and R. P. Behringer, Rev. Mod. Phys. **68**, 1259 (1996).
[10] Y. Amarouchene and H. Kellay, Phys. Fluids **18**, 031707 (2006).
[11] J. R. Royer, E. I. Corwin, B. Conyers, A. Flior, M. L. Rivers, P. J. Eng, and H. M. Jaeger, Phys. Rev. E **78**, 011305 (2008).
[12] A. M. Walsh, K. E. Holloway, P. Habdas, and R. John, Phys. Rev. Lett. **91**, 104301 (2003).
[13] S. J. de Vet and J. R. de Bruyn, Phys. Rev. E **76**, 041306 (2007).
[14] E. C. Rericha, C. Bizon, M. D. Shattuck, and H. L. Swinney, Phys. Rev. Lett. **88**, 014302 (2001).
[15] X. Cheng, G. Varas, D. Citron, H. M. Jaeger, and S. R. Nagel, Phys. Rev. Lett. **99**, 188001 (2007).
[16] U. Tüzün and R. M. Nedderman, Chem. Eng. Sci. **40**, 325 (1985).
[17] U. Tüzün and R. M. Nedderman, Chem. Eng. Sci. **40**, 337 (1985).
[18] K. Wieghardt, Annu. Rev. Fluid Mech. **7**, 89 (1975).
[19] D. Chehata, R. Zenita, and C. R. Wassgren, Phys. Fluids **15**, 1622 (2003).
[20] O. Zik, J. Stavans, and Y. Rabin, EPL **17**, 315 (1992).
[21] C. R. Wassgren, J. A. Cordova, R. Zenit, and A. Karion, Phys. Fluids **15**, 3318 (2003).
[22] K. M. Hákonardóttir and A. J. Hogg, Phys. Fluids **17**, 077101 (2005).
[23] Y. Fang, M. Gao, J. J. Wylie, and Q. Zhang, Phys. Rev. E **77**, 041302 (2008).
[24] M. Gao, J. J. Wylie, and Q. Zhang, Commun. Pure Appl. Anal. **8**, 275 (2009).
[25] J. J. Wylie, Q. Zhang, and X. X. Sun, Phys. Rev. Lett. **97**, 104501 (2006).
[26] J. J. Wylie and Q. Zhang, Phys. Rev. E **74**, 011305 (2006).
[27] J. J. Wylie, Q. Zhang, Y. Li, and X. Hengyi, Phys. Rev. E **79**, 031301 (2009).
[28] J. J. Wylie, Q. Zhang, H. Y. Xu, and X. X. Sun, EPL **81**, 54001 (2008).
[29] S. McNamara and W. R. Young, Phys. Fluids A **4**, 496 (1992).